Origin of solar surface activity and sunspots

Sarah Jabbari

Cover image: Bipolar magnetic structures.
Formation of bipolar magnetic spots at the surface in the two layer forcing in a spherical geometry.

ISBN 978-91-7649-370-0

Printed in Sweden by Holmbergs, Malmö 2016
Distributor: Department of Astronomy, Stockholm University

To those,
whom I love

Abstract

Sunspots and active regions are two of the many manifestations of the solar magnetic field. This field plays an important role in causing phenomena such as coronal mass ejections, flares, and coronal heating. Therefore, it is important to study the origin of sunspots and active regions and determine the underlying mechanism which creates them. It is believed that flux tubes rising from the bottom of the convection zone can create sunspots. However, there are still unanswered questions about this model. In particular, flux tubes are expected to expand as they rise, hence their strength weakens and some sort of reamplification mechanism must complement this model to match the observational properties of sunspots. To compensate for the absence of such an amplification mechanism, the field strength of the flux tubes, when at the bottom of the convection zone, must be far stronger than present dynamo models can explain.

In the last few years, there has been significant progress toward a new model of magnetic field concentrations based on the negative effective magnetic pressure instability (NEMPI) in a highly stratified turbulent plasma. NEMPI is a large-scale instability caused by a negative contribution to the total mean-field pressure due to the suppression of the total turbulent pressure by a large-scale magnetic field. In this thesis, I study for the first time NEMPI in the presence of a dynamo-generated magnetic field in both spherical and Cartesian geometries. The results of mean-field simulations in spherical geometry show that NEMPI and the dynamo instability can act together at the same time such that we deal with a coupled system involving both NEMPI and dynamo effects simultaneously. I also consider a particular two-layer model which was previously found to lead to the formation of bipolar magnetic structures with super-equipartition strength in the presence of a dynamo-generated field. In this model, the turbulence is forced in the entire domain, but the forcing is made helical in the lower part of the domain, and non-helical in the upper part. The study of such a system in spherical geometry showed that, when the stratification is strong enough, intense bipolar regions form and, as time passes, they expand, merge and create giant structures. To understand the underlying mechanism of the formation of such intense, long-lived bipolar structures with a sharp boundary, we performed a systematic numerical study of this model in plane parallel geometry by varying the magnetic Reynolds number, the scale separation ratio, and Coriolis number. Finally, I investigate the formation of the current sheet between bipolar regions and reconnection of oppositely orientated magnetic field lines and demonstrate that for large Lundquist numbers,

S, the reconnection rate is nearly independent of S – in agreement with recent studies in identical settings.

List of Papers

The following papers, referred to in the text by their Roman numerals, are included in this thesis.

PAPER I: **Jabbari, S.**, Brandenburg, A., Kleeorin, N., Mitra, D. & Rogachevskii, I.: 2013, "Surface flux concentration in a spherical α^2 dynamo," *Astron.& Astrophys.* **556**, A106

PAPER II: **Jabbari, S.**, Brandenburg, A., Kleeorin, N., Mitra, D. & Rogachevskii, I.: 2014, "Magnetic flux concentrations from dynamo-generated fields," *Astron.& Astrophys.* **568**, A112

PAPER III: Brandenburg, A., Gressel, O., **Jabbari, S.**, Kleeorin, N. & Rogachevskii, I.: 2014, "Mean-field and direct numerical simulations of magnetic flux concentration from vertical field," *Astron.& Astrophys.* **562**, A53

PAPER IV: **Jabbari, S.**, Brandenburg, A., Kleeorin, N., Mitra, D. & Rogachevskii, I.: 2015, "Bipolar magnetic spots from dynamos in stratified spherical shell turbulence," *Astrophys. J.* **805**, 166

PAPER V: **Jabbari, S.**, Brandenburg, A., Mitra, D., Kleeorin, N. & Rogachevskii, I.: 2016, "Turbulent reconnection of magnetic bipoles in stratified turbulence," *MNRAS*, In press, arXiv:1601.08167

My Contribution to the Papers

I In **Paper I**, nearly all of the mean-field simulations were performed and analyzed by me. The evaluation of the simulation results was done together with the other coauthors. I played an active role in the discussion of the content of the text and in the adaptations following the referee's reports.

II **Paper II** is a follow-up of **Paper I** and was completely conducted by me. I performed all the simulations, both the direct numerical simulations (DNS) and the mean-field simulations (MFS) and produced all plots of the paper. I wrote some sections in the paper, although they were largely rewritten and extended by the senior coauthors.

III My contribution to **Paper III** was mostly through running both MFS and DNS. Findings from these simulations were then more rigorously analyzed by Axel, who also wrote most of the text of the paper. I also participated in the analysis of the results and produced some plots and tables of the paper.

IV In **Paper IV**, I did some work on the implementation of the setup and developed some analysis tools in the PENCIL CODE and wrote corresponding IDL routines. I did most of the analysis and made all the plots and tables used in the paper. I also wrote the first complete version of the text, which was later improved by the coauthors.

V **Paper V** is a follow-up of **Paper IV** and was completely conducted by me. I did all the runs related to the paper, all the analysis and plots and I wrote new codes with IDL. I also wrote all the text except for some suggested additions and comments by the coauthors.

Contents

1. The magnetic Sun

Darkness must pass
A new day will come
And when the sun shines
It will shine out the clearer.

J.R.R. Tolkien

The Sun, the star of our solar system, plays a crucial role in the existence of life on Earth. It is also very important for a broad range of scientific problems because it is the closest astrophysical laboratory that one can use to study plasma and different models of magnetohydrodynamic (MHD) and MHD turbulence. The Sun is a small yellow star (G type), which constitutes 98.8% of the mass of our solar system. It is 1.5×10^{11} m away from Earth, and it takes approximately 8 minutes and 30 seconds for its light to reach the Earth. For comparison, light from any nearest neighboring star takes about 4.2 years to reach Earth. This difference illustrates that our ability to study surface structures on the nearest start, our Sun, is unique. This giant ball of hot gas has differential rotation in the sense that its equator rotates faster than its poles. Like many other stars, the Sun has a global magnetic field and an activity cycle. Solar activity varies over an 11-year cycle, changing from a quiet solar minimum to an active solar maximum. The Sun has an interior and an atmosphere. The solar interior consists of three layers, the core, the radiative interior, and the convection zone. The solar atmosphere can be described as consisting of four layers, the photosphere, the chromosphere, the transition region, and the corona (see Figure 1.1). In this chapter, I will give a brief description of the solar structure, its activity, and its magnetic field. Then, I will discuss reconnection of magnetic field in the Sun and will present a summary of solar observations and techniques.

1.1 Solar structure

The radiated energy flux of the Sun is produced in the core where nuclear reactions consume hydrogen to form helium through proton–proton reaction chains and the so-called carbon–nitrogen–oxygen cycle. These reactions release the energy that in the end leaves the surface mostly as visible light and continues to propagate toward outer space through radiation in various forms along with the solar wind. As mentioned above, the energy is produced in the core, which

has high temperature (15×10^6 K) and high density (15×10^4 kg/m^3) to prepare the condition for nuclear reactions. Outside of this layer, temperature and density both decrease such that photons can be observed and re-emitted. In other words, in this layer energy is transported through radiation. This is the reason it is called the radiation layer, which extends from 0.25 up to about 0.7 solar radii. The outermost layer of the solar interior, the convection zone, is characterized by energy transport through convection and extends from 0.7 up to one solar radii. Here, one might note that the radiation layer rotates approximately like a solid body while the convection zone has differential rotation. This leads to the formation of a very strong shear layer between these two layers, which is called the tachocline. In some theories for the origin of the solar global magnetic field, the tachocline plays an important role. We will come back to this subject later in Section 1.3. The convection zone is a layer that consists of giant upflows of hot gas, which raise up, lose their heat, and sink down. As the cool gas is darker than the hot plasma, these convective motions create patterns at the surface which are called granules.

The deepest layer of the solar atmosphere is called the photosphere. Here the density and temperature drop dramatically. In this layer, one can see fascinating features like dark sunspots, bright faculae, and granules. Over 100 years ago, it was shown that sunspots are magnetic in nature. I will get back to this later and discuss it in more detail, as it is the main subject of this thesis. In the photosphere, one can also measure the 5 minute oscillations using Doppler shifts of specific lines. The study of the Sun using waves and oscillations is called helioseismology. I will give a brief description of this method in Section 1.5. The chromosphere is the layer above the photosphere where the temperature rises gradually from 6000 K to about 20,000 K. This increase of temperature continues through a thin layer called the transition region, where the temperature reaches up to a few million Kelvin. The Sun's outer atmosphere, which is visible during total eclipses is called the corona (Stix, 1989).

The solar atmosphere has been subject to many numerical and observational studies (see Kiselman, 2001; de la Cruz Rodríguez et al., 2011; Henriques and Kiselman, 2013; Leenaarts et al., 2015; Carlsson et al., 2015; Golding et al., 2016). In particular, Kiselman (2008) confronted three-dimensional solar photospheric models with observation. Later, Kiselman et al. (2011) studied the possibility of a latitudinal dependence of the solar spectrum.

The corona has a high temperature, which cannot be explained by radiative heat transfer from the lower layers of the Sun. Thus, the coronal heating process is the main question concerning the solar corona (Aschwanden, 2004). There have been many studies proposing different mechanisms responsible for this phenomenon, e.g., heating by dissipation of magnetohydrodynamic waves,

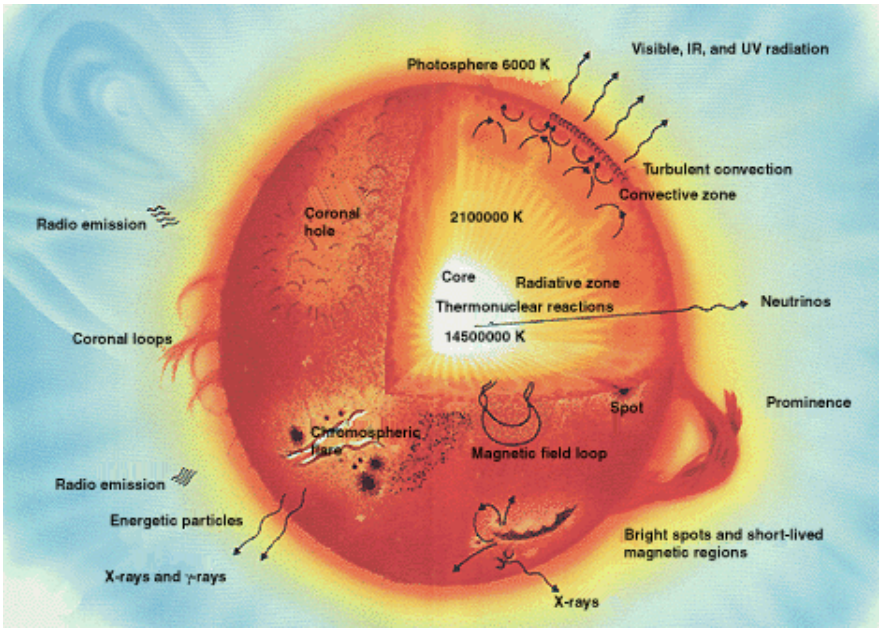

Figure 1.1: The solar structure. Courtesy of NASA.

reconnection of the magnetic field lines, and nanoflares. However, the mechanism behind the heating of the corona is still under debate (see Klimchuk, 2015).

Finally, let me end this section with a comment on the solar wind. It contains accelerated plasma particles whose velocity depend on many factors and varies from 400 up to 900 km/s. The interaction of the solar wind with the planetary magnetic field can create magnetic storms, and aurorae (northern lights). The solar wind provides good examples of MHD plasma turbulence. Yordanova et al. (2009) investigated solar wind turbulence using Ulysses magnetic field data at times of different solar activity levels, different heliospheric latitudes, and various distances from the disk center. Their results show that the properties of the magnetic field turbulence depends on the regions, heliographic latitude, distance and also level of solar activity; see also (Perri et al., 2009; Yordanova et al., 2011; Greco et al., 2015).

1.2 Solar activity and sunspots

As mentioned in the previous section, the Sun has a magnetic field which manifests itself by surface features like sunspots and active regions.

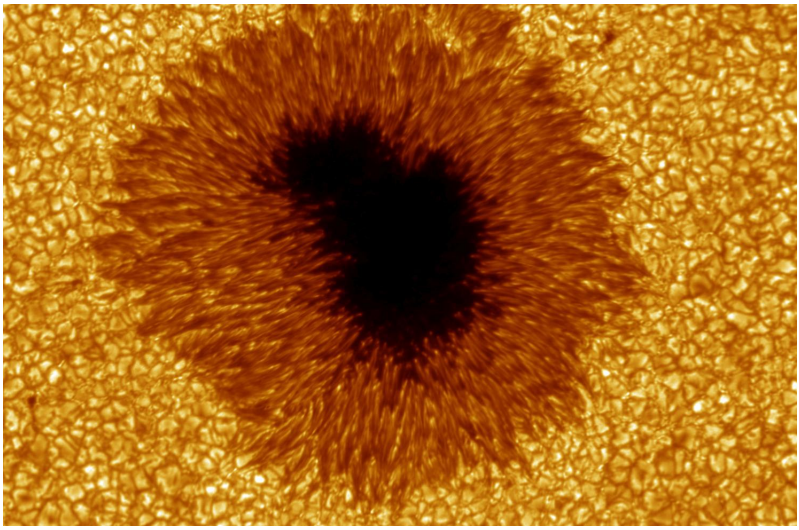

Figure 1.2: Image of a sunspot associated with AR 397 and observed with the Swedish Solar Telescope (SST) at wavelength 630.2 nm (Fe I) on 3th July 2003. Observation by Dan Kiselman and image processing by Mats Löfdahl.

1.2.1 Sunspots

Sunspots are areas of a strong magnetic field concentrations (with field strengths of a few kG), which look darker than their surroundings on the solar surface. Their darkness is due to a strongly reduced radiative flux caused by the suppression of convection by the magnetic field. This results in the dark appearance of sunspots (see Figure 1.2). Sunspots usually have sizes in the range 5 to 50 Mm and lifetimes from a fraction of a day up to three months. These features are typically confined to an equatorial belt, the activity belt, which is between the equator and ± 35 degrees latitude (Solanki, 2003). A sunspot consists of two parts, a dark part (umbra) and a brighter part (penumbra), which surrounds the umbra (see Figure 1.2). There have been many studies on the penumbra part of the sunspots using both models and observations. Scharmer et al. (2011) studied a sunspot penumbra using imaging spectropolarimetric data from the Swedish 1-meter Solar Telescope, and reported the existence of convective downward flows of up to 1 km/s, demonstrating that the penumbra is fully convective.

Figure 1.3 shows a magnetogram of the Sun. The black and white shades show the two polarities of the magnetic field in active regions and sunspots. The magnetic nature of sunspots was first reported by Hale (1908). He used the Zeeman effect and studied the spectrum of sunspots and compared it with that from a portion of the Sun without a sunspot (not very far from the spot).

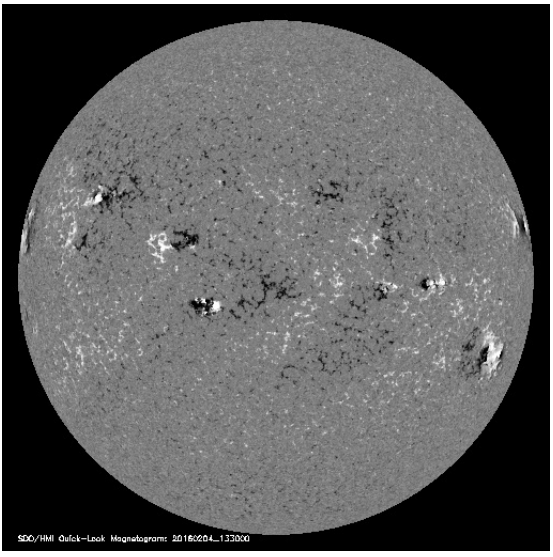

Figure 1.3: A full disk Magnetogram image of the Sun taken by SDO/HMI on 4/02/2016.

According to the Zeeman effect, when a gas is placed in a magnetic field, most of its spectral lines split into several components. The separation between lines is directly proportional to the strength of the magnetic field, so by measuring the amount of split one can estimate the strength of the magnetic field (Mestel, 1999). Hale showed that the Zeeman effect exists also in the spectrum of sunspots and that sunspots, therefore must have strong magnetic fields.

1.2.2 Solar activity

The number and spatial distribution of sunspots and active regions varies with an eleven year cycle. This can be seen from the so-called butterfly diagram, which is often shown as a contour plot of the magnetic field in the latitude-time plane (see Figure 1.4). The name of this diagram is taken from the first similar diagram constructed by Edward Maunder in 1904, which was a cumulative diagram of all the spots in the latitude–time plane. As mentioned earlier, sunspots tend to appear in the activity belt. At the beginning of a new solar cycle, sunspots appear at high latitudes, but as the cycle progresses toward its maximum (when there are many sunspots and active regions) the spots form at lower latitudes. The minimum of the cycle is defined as the time when the number of sunspot on the surface of the Sun is minimum. Later, when a new cycle starts, sunspots appear again at high latitudes. This behavior of the sunspot number and their location leads to the butterfly like pattern on the

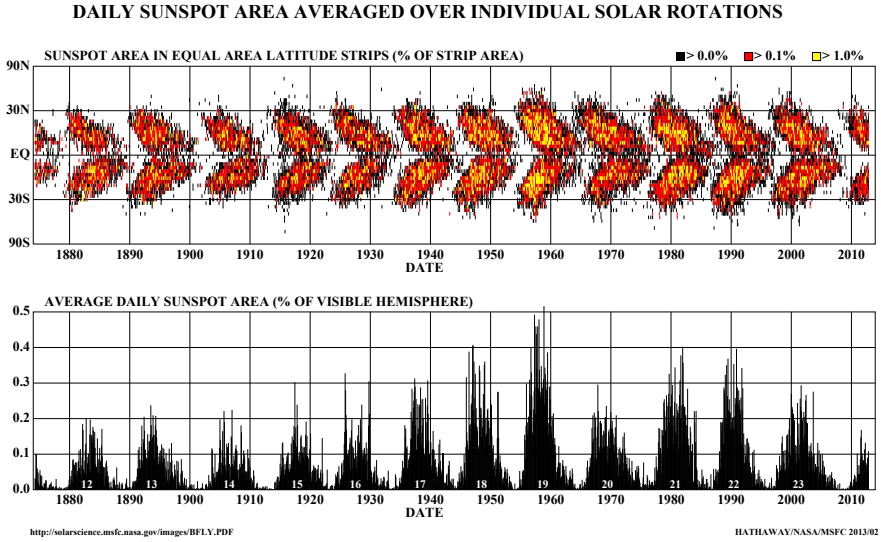

Figure 1.4: Upper panel: the position of the sunspots on the latitude-time plane. Lower panel: the averaged daily sunspots area versus time. The figure was taken from the NASA Marshall Space Flight center for Solar Physics.

latitude-time plot. Thus, this plot is called butterfly diagram.

1.3 Solar magnetic field

Before discussing the origin of sunspots and active regions it is useful to present a brief summary of the origin of the solar global magnetic field. According to the theory of stellar structure, the outer 30% of Sun by radius is unstable due to convection. It was also suggested that the turbulent convection could convert kinetic energy to magnetic energy partially through dynamo action. A dynamo usually needs a weak initial seed field, which grows exponentially in time, undergoes a non-linear phase and then saturates after reaching some level of strength. According to the dynamo theory, the magnetic field strength can grow by self-excitation (Brandenburg and Subramanian, 2005).

Recently, Jouve et al. (2015) performed numerical simulations of a spherical shell to study the evolution of the magnetic fields of a differentially rotating

stars. Their main focus was to investigate the magnetic fields of the radiative zone in such stars and to study the possibility of magnetic instabilities like magneto-rotational instability (MRI) and Taylor instability (Tayler, 1973; Spruit, 2002). Their result showed that indeed MRI occurs in the unstratified spherical shell with strong differential rotation; see also (Gaurat et al., 2015).

In the next section, I will briefly explain dynamo theory using the mean-field approach.

1.3.1 Dynamo theory

In the Sun, toroidal and poloidal magnetic fields can act as a power source for each other. On the one hand, the stretching of the poloidal field due to the differential rotation leads to the creation of a toroidal field and, on the other hand, the effect of helical turbulence on the toroidal field produces a poloidal field (Parker, 1955b). Figure 1.5 is a simple illustration of a dynamo process, which includes stretching, twisting, folding, and merging of a flux tube.

The two equations, which play an important role in the formulation of a fully nonlinear dynamo are the momentum and induction equations:

$$\rho \frac{\mathrm{D}\boldsymbol{U}}{\mathrm{D}t} = -\nabla p + \boldsymbol{J}\times\boldsymbol{B} + \rho\boldsymbol{g} + \rho\nu\left(\nabla^2\boldsymbol{U} + \frac{1}{3}\nabla(\nabla\cdot\boldsymbol{u}) + 2\mathsf{S}\cdot\nabla\ln\rho\right), \quad (1.1)$$

$$\frac{\partial\boldsymbol{B}}{\partial t} = \nabla\times(\boldsymbol{U}\times\boldsymbol{B}) + \eta\nabla^2\boldsymbol{B}, \quad (1.2)$$

where ν and η are kinematic viscosity and magnetic diffusivity, respectively, both are here assumed to be constant, and S is the traceless rate-of-strain tensor of the flow.

Here, I follow the mean-field approach, where one assumes that all dependent variables are written in the form of a mean and a fluctuating part. One should note that this assumption is different from perturbation theory because we do not impose any restriction on the strength of the fluctuating part. By applying mean-field theory to the induction equation, we are able to consider the effect of turbulence on the magnetic field fluctuation by introducing the mean electromotive force.

But, before getting there, let me give a brief description of turbulence as it plays an important role in the studies of this thesis. A turbulent flow is opposite to a laminar flow. When a flow is turbulent, its characteristics, e.g. the velocity, change rapidly in space and time. In fact, in turbulence, the inertial forces overcomes the viscosity of the flow. In this context, a dimensionless quantity, the fluid Reynolds number, is defined as the ratio of momentum forces to viscous forces,

$$\mathrm{Re} = ul/\nu. \quad (1.3)$$

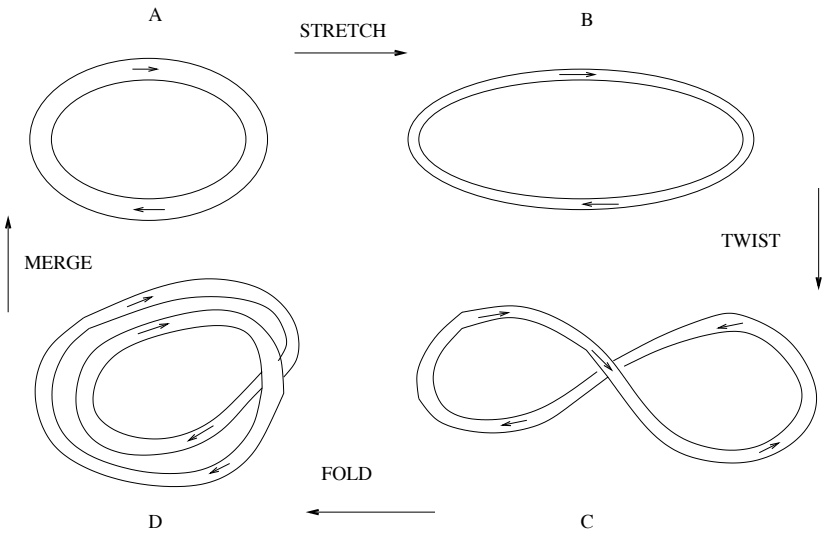

Figure 1.5: An illustration of a stretch-twist-fold dynamo taken from Brandenburg and Subramanian (2005).

In our simulations, when the turbulence is driven by forcing, u is taken to be the root mean square velocity, $u_{\rm rms}$, and l is a typical length scale of turbulent eddies. In forced turbulence, this length scale is replaced by $1/k_{\rm f}$, where $k_{\rm f}$ is the forcing wavenumber. In the case of small Reynolds numbers, we deal with a laminar flow, where the viscous forces are dominant and Re is large for a turbulent flow. In numerical simulations with high Reynolds number (turbulent flows), one needs large grid resolution to resolve a broad range of scales. This is numerically very expensive and memory consuming. Therefore, to perform realistic simulations of the Sun with Reynolds number of about 10^{11}, one needs to have access to much stronger computing sources than what will be possible in the foreseeable future.

Now, let me return to the mean-field approach and introduce the Reynolds decomposition:

$$\boldsymbol{B} = \overline{\boldsymbol{B}} + \boldsymbol{b}, \tag{1.4}$$

$$\boldsymbol{U} = \overline{\boldsymbol{U}} + \boldsymbol{u}, \tag{1.5}$$

where $\overline{\boldsymbol{B}}$ and $\overline{\boldsymbol{U}}$ are the mean values and $\boldsymbol{b}$ and $\boldsymbol{u}$ are the fluctuations. In the next section I will explain how dynamo theory describes the large-scale α^2 dynamo.

1.3.2 α^2 dynamo

We substitute equation (1.4) and equation (1.5) into equation (1.2), and then take the average of this equation using the Reynolds averaging rules, so we obtain:

$$\frac{\partial \overline{\boldsymbol{B}}}{\partial t} = \nabla \times (\overline{\boldsymbol{U}} \times \overline{\boldsymbol{B}}) + \eta \nabla^2 \overline{\boldsymbol{B}} + \nabla \times \overline{\mathcal{E}}, \tag{1.6}$$

where $\overline{\mathcal{E}} = \overline{\boldsymbol{u} \times \boldsymbol{b}}$. For isotropic turbulence and under the assumption of perfect scale separation, the mean electromotive force (EMF) is given by (Moffatt, 1978; Krause and Rädler, 1980)

$$\overline{\mathcal{E}} = \alpha \overline{\boldsymbol{B}} - \eta_{\mathrm{t}} \nabla \times \overline{\boldsymbol{B}}. \tag{1.7}$$

This expression implies that for a non-zero α effect, the α^2 dynamo can generate a mean magnetic field depending on boundary conditions, the size of the domain, and the value of turbulent magnetic diffusivity. One can determine these coefficients using the concept of kinetic helicity for isotropic turbulence,

$$\alpha \approx \alpha_0 \equiv -\tfrac{1}{3} \tau \overline{\boldsymbol{\omega} \cdot \boldsymbol{u}}, \quad \eta_{\mathrm{t}} \approx \eta_{\mathrm{t}0} \equiv \tfrac{1}{3} \tau \overline{\boldsymbol{u}^2}, \tag{1.8}$$

where $\boldsymbol{\omega} = \nabla \times \boldsymbol{u}$ is the vorticity, $\tau = (u_{\mathrm{rms}} k_{\mathrm{f}})^{-1}$ is an estimate of the correlation time, and k_{f} is the wavenumber of the energy-carrying eddies (or forcing wavenumber in forced turbulence). There is also a numerical approach called a test-field method, by which one can measure these coefficients. I present a brief description of this method in Section 1.3.3.

By substituting equation (1.7) into equation (1.6), we get

$$\frac{\partial \overline{\boldsymbol{B}}}{\partial t} = \nabla \times (\overline{\boldsymbol{U}} \times \overline{\boldsymbol{B}}) + \eta \nabla^2 \overline{\boldsymbol{B}} + \nabla \times (\alpha \overline{\boldsymbol{B}}) - \nabla \times (\eta_{\mathrm{t}} \nabla \times \overline{\boldsymbol{B}}). \tag{1.9}$$

We consider the case when there is no mean flow ($\overline{\boldsymbol{U}} = 0$) and the turbulence is homogeneous. This implies that α and η_{t} are constants. It is therefore straightforward to write the mean induction equation in the form

$$\frac{\partial \overline{\boldsymbol{B}}}{\partial t} = \eta_{\mathrm{T}} \nabla^2 \overline{\boldsymbol{B}} + \alpha \nabla \times \overline{\boldsymbol{B}}, \tag{1.10}$$

where

$$\eta_{\mathrm{T}} = \eta + \eta_{\mathrm{t}} \tag{1.11}$$

is total magnetic diffusivity. We search for the real part of an exponentially growing solution of equation (1.10):

$$\overline{\boldsymbol{B}}(\boldsymbol{x}, t) = \hat{\boldsymbol{B}}(\boldsymbol{k}) e^{i\boldsymbol{k}\cdot\boldsymbol{x} + \lambda t}. \tag{1.12}$$

Substituting this expression into the mean induction equation, we get

$$\lambda \hat{\boldsymbol{B}} = \alpha i \boldsymbol{k} \times \hat{\boldsymbol{B}} - \eta_T k^2 \hat{\boldsymbol{B}}. \tag{1.13}$$

The dispersion relation is then

$$(\lambda + \eta_T k^2)\left((\lambda + \eta_T k^2)^2 - \alpha^2 k^2\right) = 0, \tag{1.14}$$

which yields the growth rate of the α^2 dynamo as

$$\lambda = -\eta_T k^2 + |\alpha k|. \tag{1.15}$$

We use a parameter called the dynamo number to characterize the α^2 dynamo. The dynamo number is defined as

$$C_\alpha = \alpha / \eta_{\rm T} k_1, \tag{1.16}$$

where α is a typical value of the α effect, and k_1 is the lowest wavenumber of the magnetic field that can be fitted into the domain. We also define another parameter called the normalized kinetic helicity,

$$\varepsilon_{\rm f} \equiv \overline{\boldsymbol{\omega} \cdot \boldsymbol{u}} / k_{\rm f} u_{\rm rms}^2. \tag{1.17}$$

In a stratified rotating system, kinetic helicity is produced self-consistently by the interaction between rotation (represented by the angular velocity, Ω) and stratification (represented by the gravitational acceleration g). In such a case, a relation between kinetic helicity and Coriolis number, ${\rm Co} = 2\Omega / u_{\rm rms} k_{\rm f}$, was suggested in the form of (Blackman and Brandenburg, 2002; Brandenburg et al., 2012b; Candelaresi and Brandenburg, 2013; Losada et al., 2013)

$$\varepsilon_{\rm f} \equiv \varepsilon_{\rm f0}\, {\rm Gr}\, {\rm Co} \quad ({\rm for}\ {\rm Gr}\, {\rm Co} \lesssim 0.1). \tag{1.18}$$

Here, Gr is the gravitational parameter, which is defined by

$${\rm Gr} = g / c_{\rm s}^2 k_{\rm f}, \tag{1.19}$$

where $c_{\rm s}$ is the sound speed. Combining equations (1.16) and (1.19), the dynamo number takes the form

$$C_\alpha = -\varepsilon_{\rm f0}\, {\rm Gr}\, {\rm Co}\, k_{\rm f} / k_1. \tag{1.20}$$

This expression indicates that the combination of stratification and rotation leads to an α effect. This result was confirmed through direct numerical simulations (DNS) of Losada et al. (2013) and in **Paper II**.

In mean field simulations (MFS) of **Paper I**, we assumed an additional ad hoc nonlinearity called α quenching. This means that α is then replaced by

$$\alpha = \frac{\alpha_0}{1 + Q_\alpha \overline{\boldsymbol{B}}^2 / B_{\rm eq}^2}. \tag{1.21}$$

The larger the quenching parameter Q_α, the smaller is the magnetic field resulting from the α effect. Here, we have used the equipartition magnetic field strength, $B_{\rm eq} = \sqrt{\overline{\rho}}\, u_{\rm rms}$ to normalize the magnetic field.

Similar to the induction equation (1.6), there are also mean-field parameterizations for the mean momentum equation equation (1.1). It has the form

$$\rho \frac{{\rm D}\overline{\boldsymbol{U}}}{{\rm D}t} = -\nabla p + \rho \boldsymbol{g} + \overline{\boldsymbol{F}}_{\rm M} + \overline{\boldsymbol{F}}_{\rm K}, \tag{1.22}$$

where p is the gas pressure, $\overline{\boldsymbol{F}}_{\rm K} = \rho \nu_{\rm t} (\nabla^2 \overline{\boldsymbol{U}} + \frac{1}{3} \nabla \nabla \cdot \overline{\boldsymbol{U}} + 2 \overline{\mathsf{S}} \nabla \ln \overline{\rho})$ is the viscous force of the mean flow (used in all mean-field and large eddy simulations), while $\overline{\boldsymbol{F}}_{\rm M}$ is the mean Lorentz force, which can be expressed as

$$\overline{\boldsymbol{F}}_{\rm M} = \overline{\boldsymbol{J}} \times \overline{\boldsymbol{B}} + \frac{1}{2\mu_0} \nabla (q_{\rm p0} \overline{\boldsymbol{B}}^2) + ..., \tag{1.23}$$

where μ_0 is the vacuum permeability, and dots refer to neglected terms (Kleeorin et al., 1990; Brandenburg et al., 2012a; Käpylä et al., 2012). Here, the second term represents one of the most important turbulent contributions to the mean Lorentz force. This will be discussed in detail in Section 2.2.

1.3.3 Test-field method

The test-field method (TFM) is a numerical technique to calculate the dynamo coefficients α_{ij} and η_{ij}. In TFM, we employ different independent vector magnetic fields called test fields and replace them in equation (1.6), while the velocity field is taken from the simulations (Schrinner et al., 2005; Brandenburg, 2005; Schrinner et al., 2007; Brandenburg et al., 2010a). Then, we calculate $\overline{\boldsymbol{\mathcal{E}}}$ and, using equation (1.7), we obtain a system of equations, which can be solved for the coefficients α_{ij} and η_{ij}. For more detail on TFM see Jabbari (2014b).

In **Paper II**, we performed simulations with TFM to calculate the dynamo coefficients for stratified turbulent plasma in the presence of the rotation (see Section 3.2.2).

1.4 Magnetic reconnection

Magnetic reconnection is a fundamental plasma process, which occurs in different astrophysical environments and is defined as a reconfiguration of the

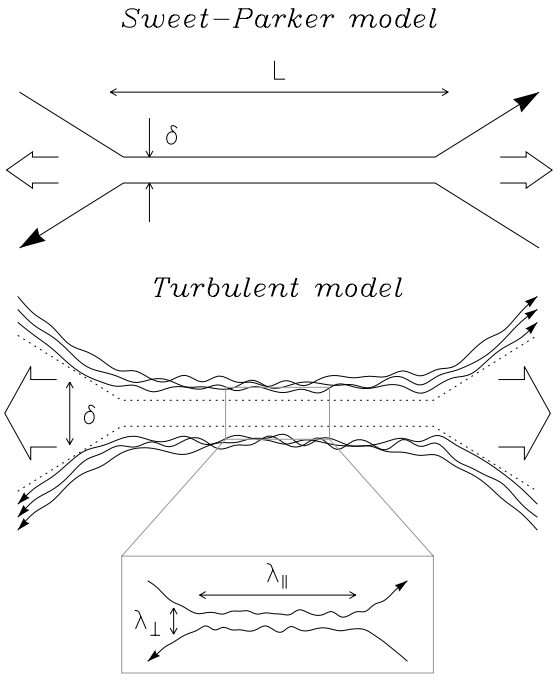

Figure 1.6: A schematic sketch of a reconnecting field lines for Sweet-Parker (upper panel) and turbulent reconnection (lower panel) taken from Kowal et al. (2009).

magnetic field lines which. This causes the conversion of magnetic energy to thermal energy, kinetic energy, and even particle acceleration. Reconnection occurs on a timescale between the resistive diffusion and Alfvén timescales and leads to a change of the magnetic field topology. Reconnection also happens in the Sun and is believed to play an important role in different phenomena like solar flares, coronal mass ejections, and coronal heating (Zweibel and Yamada, 2009). A classical model of reconnection was suggested by Parker (1957) and Sweet (1958), known as Sweet-Parker theory of reconnection. According to their model, the reconnection rate depends on the magnetic diffusivity of the plasma. This implies that for a very small value of magnetic diffusivity (astrophysical plasma), the Sweet-Parker reconnection rate should go to zero. Hence, to explain the reconnection process in the astrophysical phenomena, one needs to adopt a model where the reconnection rate is independent of magnetic diffusivity, i.e., one needs to consider turbulent reconnection.

Figure 1.6 presents a sketch of classical reconnection (upper panel) and turbulent reconnection (lower panel).

1.4.1 Classical reconnection

According to the Sweet-Parker (SP) theory of reconnection, the rate of reconnection, $v_{\rm rec}$, depends on the magnetic diffusivity though a dimensionless parameter known as the Lundquist number, S. This number is defined as

$$S = v_{\rm A} L/\eta, \tag{1.24}$$

where $v_{\rm A} = B/\sqrt{\mu_0 \rho}$ is the Alfvén velocity and L is the typical length scale (length of the current sheet). According to the SP theory, the rate of reconnection is

$$v_{\rm rec} = v_{\rm A} S^{-1/2}. \tag{1.25}$$

1.4.2 Fast reconnection

As mentioned above, for the regime of large Lundquist numbers, relevant to astrophysical plasmas, different models of reconnection have been proposed. In a model suggested by Lazarian and Vishniac (1999), hereafter LV99, for large Lundquist numbers, and in the presence of turbulence, $v_{\rm rec}$ is independent of S. Such reconnection is known as turbulent or fast reconnection. Fast reconnection has been studied in DNS of turbulent magnetohydrodynamics (MHD) in both two and three dimensions (Loureiro et al., 2009; Kowal et al., 2009; Huang and Bhattacharjee, 2010; Loureiro et al., 2012; Beresnyak, 2013; Oishi et al., 2015). According to LV99, the rate of the reconnection is given by

$$v_{\rm rec} \sim v_{\rm A} M_{\rm A}^2, \tag{1.26}$$

where $M_{\rm A} = u_{\rm rms}/v_{\rm A}$ is the Alfvén Mach number.

Another model of reconnection suggested by Loureiro et al. (2009), Huang and Bhattacharjee (2010), and Beresnyak (2013) predicts that for spontaneous magnetic reconnection, the reconnection rate for $S > 10^4$ is of the order of

$$v_{\rm rec} \sim (1-3) \times 10^{-2} v_{\rm A}. \tag{1.27}$$

1.4.3 Reconnection rate

To determine $v_{\rm rec}$, one can use two approaches. In one approach, the value of the inflow in the vicinity of the current sheet can be used as an estimate of the reconnection speed. In a turbulent plasma, on the other hand, one can use a more general and accurate method. In this approach, one can use Ohm's law:

$$\eta \mu_0 \boldsymbol{J} = \boldsymbol{E} + \boldsymbol{U} \times \boldsymbol{B}, \tag{1.28}$$

so that the rate of the reconnection speed, $v_{\rm rec}$ can be determined as $v_{\rm rec} \simeq v_E$, where

$$v_E = \frac{|\langle \boldsymbol{E} \rangle|}{|\langle \boldsymbol{B} \rangle|} = \frac{|\eta \langle \mu_0 \boldsymbol{J} \rangle - \langle \boldsymbol{U} \times \boldsymbol{B} \rangle|}{|\langle \boldsymbol{B} \rangle|}. \tag{1.29}$$

Here, v_E is measured in the vicinity of the current sheet and angle brackets denote averaging along the x and z directions, where z is along the largest side of the current sheet, i.e., perpendicular to the electric current (see Figure 1.6).

1.4.4 Reconnection in the Sun

In a magnetized plasma, when two flux tubes are entangled, the magnetic energy can be changed by two processes, either by a slow decay on a resistive time scale or by the change of the topology due to reconnection. In the limit of high magnetic Reynolds numbers (the ratio of advection to diffusion terms in the induction equation), only the latter will have an effect on sub-resistive timescales. In the Sun with its high magnetic Reynolds number, we observe similar effects, where two magnetic flux tubes can be interlocked and therefore reconnect. Magnetic reconnection occurs during solar flares, coronal mass ejections (CMEs), and it is believed that reconnection plays an important role in heating the corona as was demonstrated recently by Chatterjee et al. (2016). The current picture suggests that in the Sun, kinetic helicity drives the dynamo, which leads to the generation of helical magnetic fields. These helical fields rise to the corona, reconnect, create eruptive events, and release energy as heat and energetic particles. One other more familiar type of reconnection is the one, which occurs due to the interaction of the solar wind with planetary magnetospheres and also in their magnetotails. These phenomena are important in the formation of aurorae or northern lights (Zweibel and Yamada, 2009).

1.5 Solar observations

Nowadays we have access to data of different ground- and space-based telescopes from different layers of the solar atmosphere. By analyzing these data, one can measure the line-of-sight velocity (using the Doppler effect), determine the magnetic field (using the Zeeman effect), and obtain the element abundance (using the absorption spectrum). However, our observations in visible light are limited to a geometrical depth where the optical depth is unity. Therefore, below the surface, it is only local and global helioseismology that can give information about the flow properties.

In this section I will present a brief summary of solar studies using optical and helioseismological techniques with a focus on surface phenomena like sunspots and active regions.

1.5.1 The Sun through the telescope

In the past few decades, there has been significant improvement in the field of observational solar physics. From the successful space missions like SOHO, TRACE, STEREO, Hinode, SDO, and IRIS to the ground based solar telescopes like the Swedish 1-meter Solar Telescope (SST), Big Bear Solar Observatory, the Atacama Large Millimeter/submillimeter Array (ALMA), and many others, we could study the Sun in different wavelengths and various time intervals. In the near future, the full utilization of ALMA and the completion of the Daniel K. Inouye Solar Telescope (DKIST) in 2018 and, after that, hopefully the European Solar Telescope (EST), are likely to lead to a new era in observational solar physics.

Concerning the actual formation process of active regions and sunspots, Getling et al. (2016) analyzed data from Hinode to study magnetic field and velocity vectors of a growing sunspot group. Their results suggest that there is a correlation between horizontal and vertical components of the magnetic field, which is inconsistent with what one expects from the rising flux tube model. According to the flux tube model, a rising flux tube leads to the emergence of a strong horizontal magnetic field with the same scale as the emerging active region. The results of Getling et al. (2016) did not show such a pattern. I will describe the rising flux tube model later in Section 2.1.

A lot can be learnt also by comparison with starspots. Piskunov and Kochukhov (2002) developed a magnetic Doppler imaging code to measure the magnetic field distribution on the surface of stars, along with chemical abundances, using polarization measurements in line profiles; see also (Kochukhov and Piskunov, 2002; Kochukhov et al., 2002).

1.5.2 Helioseismology

Helioseismology helps scientists to improve their knowledge about the interior of the Sun (see Figure 1.7). For instance, studying the internal angular velocity and its dependence on solar radius and latitude are some of the highlights of global helioseismology. Also, it became possible to determine rather accurately the depth of the convection zone – independently of stellar models that rely on realistic opacities. As mentioned before, local helioseismology gives us information about turbulent flow properties below the surface. One can use these properties to investigate the underlying mechanism of sunspot formation and even use it to predict these phenomena (Ilonidis et al., 2011; Singh et al., 2016). There are different local helioseismic methods, which have been developed; see (Schad et al., 2015) for review. Every one of them has its advantages and difficulties and so they are used for different problems.

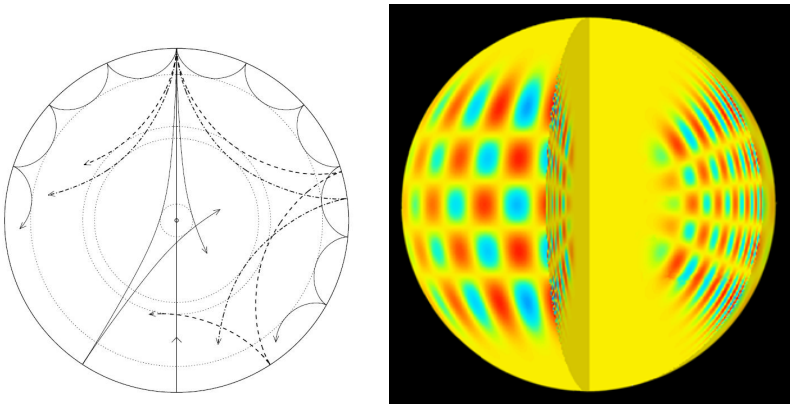

Figure 1.7: Left panel: a simplified illustration of the refracting sound waves Christensen-Dalsgaard (2003). Right pane: a three-dimensional presentation of pressure (p) modes of oscillations.

Time-distance helioseismology is one of them. In this method, spatio-temporal properties of the wave are used to measure the travel times of the sound waves between two different points on the solar surface. This method is used mostly for the investigation of supergranulation beneath the solar surface. Holography is another seismological technique, which is very close to time-distance method, but in this method one uses forward and backward propagating waves. Direct modeling, ring diagram analysis (based on local power spectra) and the Fourier-Hankel method are other helioseismic techniques. A fairly complete explanation of all these methods and their applications is given in a review by Gizon et al. (2010).

2. Models of sunspot formation

Even the smallest person
can change the course of the future.

Galadriel

In this chapter we will review different models suggested for the formation of sunspots and active regions on the solar surface. One of these approaches is based on the rising magnetic flux tube model. In the next section, I will explain briefly the basics of this model and will present a summary of the studies based on this approach. Another model, which was proposed more recently, is based on the effect of the large-scale mean magnetic field on the turbulent pressure. In this approach, the suppression of the total turbulent pressure by a large-scale magnetic field leads to a negative contribution to the effective (large-scale) magnetic pressure (the sum of turbulent and non-turbulent contributions). In the presence of strong stratification, this causes an instability, known as the negative effective magnetic pressure instability (NEMPI). I will explain the main idea behind this model in Section 2.2 and will present a brief review of past research based on this model. Later in Chapter 3, I will get back to this model and discuss the studies that we have performed in our first three papers to improve this model. In the last section of this chapter, I will discuss other alternatives for the formation of the bipolar regions and sunspots. In this context, we introduce a two-layer model, which will be discussed in more detail later in Chapters 4 and 5.

2.1 Rising flux tubes

The idea of a rising flux tube was first proposed by Parker (1955a) and is based on magnetic buoyancy. According to this model, when a magnetic flux tube forms, the total pressure (sum of the gas and magnetic pressure) would increase inside the tube due to the magnetic field. To satisfy horizontal pressure balance, the density of the tube must decrease, which makes the tube lighter than its surrounding and results in the rising of the flux tube (see Figure 2.1). In this model, it is believed that a dynamo produces such flux tubes near the base of the convection zone. In order that they rise coherently through the turbulent convection zone, it was proposed that the tubes possess twist (Parker, 1979). This was also confirmed by Jouve and Brun (2007) in 3D numerical MHD simulations.

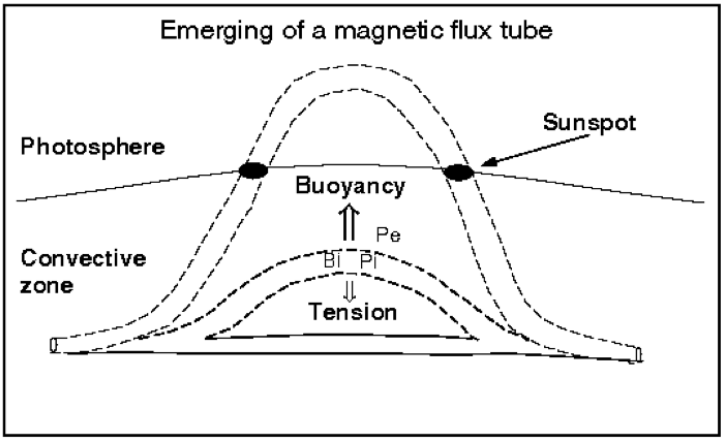

Figure 2.1: A schematic sketch of an emerging magnetic flux tube.

Later, Parker (1979) suggested that sunspots are the result of many small flux tubes in the convection zone, which rise through magnetic buoyancy and when they reach the surface, they create a single large flux tube. This is known as the cluster model of sunspot formation, which competes against the traditional monolithic picture.

In 1979, Spruit described convective collapse of small flux tubes employing Parker's idea. He used the fact that for a magnetic field larger than a critical value, the magnetic field suppresses convection (Spruit, 1979). He calculated this critical value for the convection zone and showed that it is about 1270 G at the solar surface (see also Spruit and Zweibel, 1979). Using this critical value, he divided the flux tubes into two groups, stable flux tubes with magnetic field larger than the critical value and unstable ones with magnetic field less than the critical value. When the field strength is below the critical value, the instability sets in and, according to Parker, leads to downward flow, the temperature decreases, which results in magnetic field concentration in the upper layers. This is what is called the convective collapse of flux tubes (Spruit, 1979). On the other hand, if the field strength exceeds the critical value, the tube reaches a new equilibrium state with lower energy, but if the resulted magnetic field concentration is still smaller than critical value, the tube continue to sink and will disappear at the surface.

On the one hand, by using the rising flux tube theory, one is able to explain many observed properties of sunspots such as bipolarity, their east-west orientation, polarity inversion with time and latitude, sunspot group tilt angle, and their position in low latitudes (Spörer's law; see Jouve and Brun, 2009). On the other hand, there are still concerns and unsolved question related to

this model. One of these concerns arise from the fact that such flux tubes must have a very large magnetic field (100 kG) at the bottom of the convection zone where they are believed to be generated to be able to reach to the surface and create sunspots with a magnetic field of a few kG (D'Silva and Choudhuri, 1993). So far this scenario was not confirmed by simulation or observations (Fan, 2009; Guerrero and Käpylä, 2011).

2.1.1 Numerical studies of rising flux tube

A flux tube rising from the bottom of the convection zone has been studied by Jouve and Brun (2007). They have investigated adiabatically stratified convection in a spherical geometry. They performed three-dimensional simulations using the anelastic spherical harmonics (ASH) code (Clune et al., 1999; Miesch et al., 2000; Brun et al., 2004) to study the evolution of magnetic flux tubes focusing on the effects of the twist of the field lines and the rotation on the rising process. They have confirmed that flux tubes need to be sufficiently twisted in order to rise coherently through the convection zone. Furthermore, they have shown that rotation affects both the velocity of the rise and the location of the flux tubes.

In a subsequent paper, they studied the effect of turbulent convection on a rising flux tube in a spherical rotating shell model. They introduced an axisymmetric flux tube at the base of the convection zone and showed that both the initial strength of the magnetic field and the mean flow affect the flux tube. The resulting bipolar regions in this study had some of the properties of active regions, e.g., the field strength, the east-west orientation, and the twist in the bipolar structures (Jouve and Brun, 2009).

Later, a mean-field study of a flux-transport dynamo in such spherical shell model was presented by Jouve et al. (2010a,b). In their mean-field simulations, they confirmed that, using Babcock-Leighton flux transport dynamo models, one can reproduce a magnetic field which is more toroidal with increasing rotation rate. However, their result showed that the cycle period does not correlate with the rotation period when using flux transport dynamo models under the assumption of a single cell meridional flow (Jouve et al., 2010a). In their subsequent paper, they have taken into account the rise time of the flux tube and have shown that such a time delay affects the magnetic cycle and causes a modulation of the cycle amplitude (Jouve et al., 2010b).

Buoyant flux tubes have been subject of many studies by different groups. Jouve et al. (2013) performed three-dimensional numerical simulations of convective rotating spherical shells to study the formation of bipolar regions with solar sunspot properties. In their simulations, they have inserted a magnetic flux tube near the bottom of the shell such that it became buoyant only in

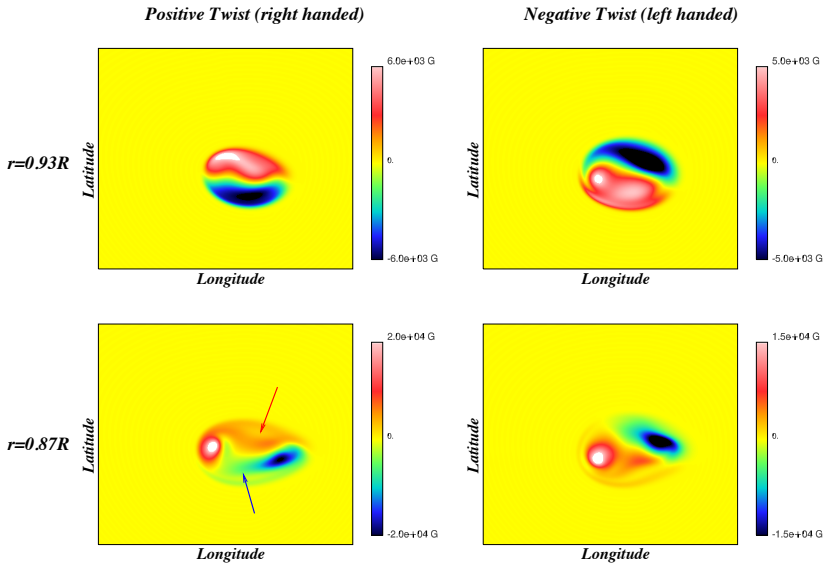

Figure 2.2: The emerging radial magnetic field at two different depth, $r = 0.93R$ (upper row) and $r = 0.87R$ (lower row), for runs with $B_0 = 10^5$ G. Taken from Jouve et al. (2013).

some parts of the full longitudinal extent. The resulting spots formed a ring-shaped structure, which is called magnetic necklace. These bipolar regions also showed a tilt angle, which was affected by the convection and differential rotation (see Figure 2.2).

Figure 2.3 shows the magnetic energy contours at $r = 0.93R$ for different simulations with different strengths of the initial magnetic field to study the asymmetry between the legs of the loop (see lines in magenta in Figure 2.3). One can see that the asymmetry decreases as the value of the initial field increases (no asymmetry for $B_0 = 2 \times 10^5$ G, last panel on the left).

Guerrero and Käpylä (2011) showed that it is possible to create flux tubes with dynamo-action in a thin shearing layer model with convection, but the maximum magnetic field strength obtained in their simulations was only a few times the equipartition field. Such a field is weaker than what is needed in the rising flux tubes approach. However, in those simulations, some of the flux tubes were able to rise up to the surface, but they expanded and weakened when they reached the surface (see Figure 2.4). One should note that in these simulations a strong deformation of the flux tubes occurs, although the Reynolds number and the density stratification are still well below realistic values for the Sun. These deformations might become worse at large values.

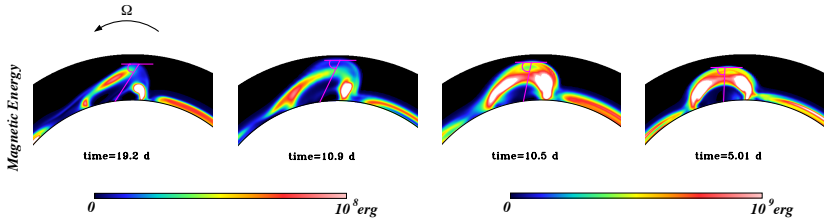

Figure 2.3: The magnetic energy color-coded at a latitude of 30° and at $r = 0.93R$ for four different runs with different values of the initial magnetic field (The value of the initial field increases from left to right). The loops are viewed downward from the north pole. Taken from Jouve et al. (2013).

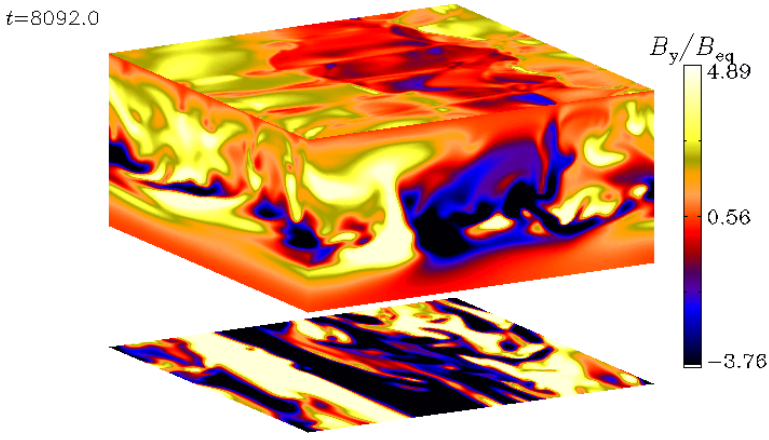

Figure 2.4: Visualization of the toroidal field (B_y) produced by dynamo-action in a thin shear layer. taken from Guerrero and Käpylä (2011).

I will return to this subject in Chapter 6, where I discuss the open questions regarding the rising flux tube model of sunspot formation.

In the last few years, there have been numerous numerical studies of flux transport models (see Cheung et al., 2008; Rempel et al., 2009; Cheung et al., 2010; Rempel and Schlichenmaier, 2011; Rempel, 2012; Rempel and Cheung, 2014). Figure 2.5 shows one of the simulation results of Rempel and Cheung (2014). As one can see from the velocity contours, there is a downflow at the position of the flux concentration. Similar downflows were observed in the case of spot formation due to NEMPI. Such downflows are discussed in **Papers III**, **IV**, and **V**.

Recently, Chatterjee et al. (2016) performed three-dimensional MHD simulations to study a flaring delta-type sunspot. In their setup, a thin cool mag-

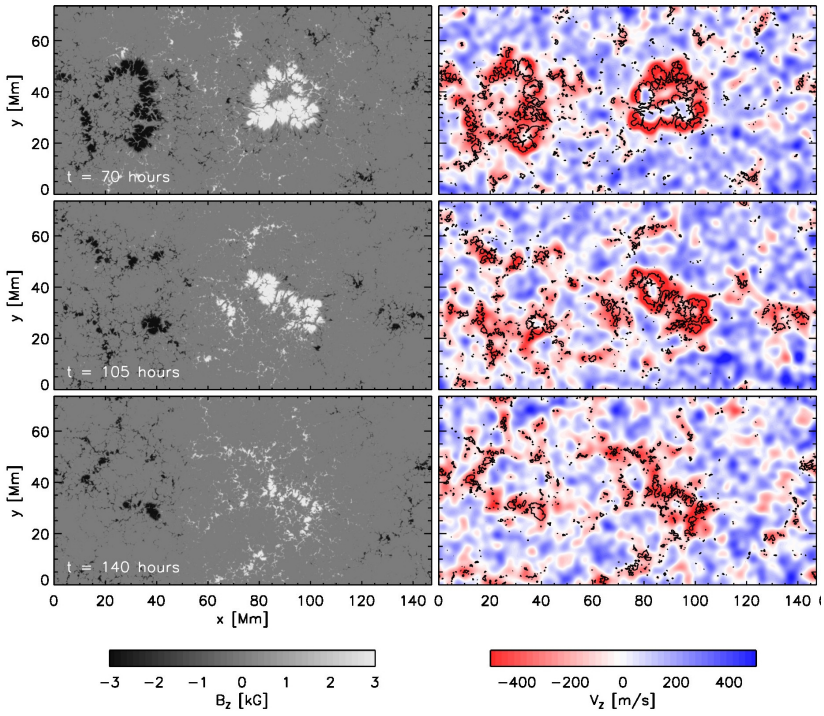

Figure 2.5: The emergence of a magnetic flux tube, simulated by Rempel and Cheung (2014).

netic layer is embedded in the lower part of the domain, which later gets unstable due to the undular instability and breaks into several flux tubes. They used an upper radiative layer which plays the role of the photosphere, which connects to an isothermal corona. They show that in such a setup, bipolar regions form as delta-sunspots. Later, this sunspot produces flares in the upper layers.

2.1.2 Fast rotating stars

Before moving on to the next model of flux concentration, let me end this section with a comment on the rising flux tube model in rapidly rotating stars. Cool stars rotate with a speed faster than the Sun. In such cases, due to the stronger Coriolis force, the flux tubes deviate from a radial ascent and move toward the pole. By comparing the path of an emerging flux tube in the Sun with a star which rotates ten times faster, one can observe that in a solar model, the flux tube moves nearly radially, while the flux tube of a rapidly rotating star emerges almost parallel to the rotation axis (Schuessler and Solanki, 1992). This leads to the formation of polar spots. Kochukhov et al. (2005) studied the

spectra of rapidly rotating (chemically peculiar) HgMn stars and showed that the mercury distribution on the surfaces of the rapidly rotating star is inhomogeneous.

Later, in Chapter 4, I will discuss polar spots (see also **Paper IV**).

2.2 Negative effective magnetic pressure instability

Kleeorin et al. (1989, 1990) proposed a different model to explain large-scale magnetic field concentrations in turbulent plasma. According to their model, the suppression of the total turbulent pressure by a large-scale magnetic field leads to a negative turbulent contribution to the total mean-field magnetic pressure, which causes the excitation of a large-scale instability (NEMPI). This instability is used as an explanation for magnetic field concentrations in the upper layer of the convection zone as the flux concentration resulting from NEMPI becomes intense in the presence of strong density stratification (Kleeorin et al., 1989, 1990, 1996). NEMPI is the main idea behind the study in our first three papers, therefore, I describe it below in more detail.

2.2.1 Effective magnetic pressure

The basic idea behind NEMPI starts from the fact that the effective magnetic pressure can be negative in a turbulent plasma. The total mean-field pressure in a turbulent plasma has the form of

$$p_{\rm tot} = p_{\rm g} + p_{\rm mag} + p_{\rm t}, \tag{2.1}$$

where $p_{\rm g}$ and $p_{\rm mag}$ are the mean gas and magnetic ($\overline{\boldsymbol{B}}^2/8\pi$) pressures, respectively [1] and $p_{\rm t}$ is the turbulent pressure, which is given by the isotropic part of the total Reynolds and Maxwell stress tensors, [2]

$$\overline{\rho}\,\overline{u_i u_j} - \frac{\overline{b_i b_j}}{4\pi} + \frac{\overline{b^2}}{8\pi}\delta_{ij} = \left(\overline{\rho}\,\overline{\boldsymbol{u}^2} - \frac{\overline{\boldsymbol{b}^2}}{4\pi} + \frac{\overline{3\boldsymbol{b}^2}}{8\pi}\right)\frac{\delta_{ij}}{3} + \ldots = \left(\underbrace{\overline{\rho}\,\overline{\boldsymbol{u}^2} + \frac{\overline{\boldsymbol{b}^2}}{4\pi}}_{\approx\text{const}} - \frac{\overline{\boldsymbol{b}^2}}{8\pi}\right)\frac{\delta_{ij}}{3} + \ldots, \tag{2.2}$$

[1] In this thesis, I use Gaussian units, while in **Papers I** and **III** we use SI units. In practice, it means that the permeability μ_0 in those papers is to be replaced by 4π. In **Papers II**, **IV** , and **V** we use nondimensional quantities which are obtained by replacing μ_0 by unity.

[2] The calculations and derivations in this section have been taken from my licentiate thesis (Jabbari, 2014b).

where dots refer to additional anisotropic parts of these stress tensors. The first expression in the right-hand side of the equation shows that, when the total energy density of the turbulence is approximately conserved (for weakly non-uniform mean magnetic field), the turbulent pressure *decreases* with increasing $\overline{\boldsymbol{b}^2}$. Kleeorin et al. (1989, 1990) formulated this in the form of

$$p_{\rm t} = E_{\rm m}/3 + 2E_{\rm k}/3. \tag{2.3}$$

Here $E_{\rm m} = \overline{b^2}/8\pi$ is the magnetic fluctuation energy density and $E_{\rm k} = \overline{\rho}\,\overline{u^2}/2$ is kinetic energy density. Once again, we assume that the total energy density of the turbulence is approximately conserved ($E_{\rm tot} = E_{\rm m} + E_{\rm k} \approx$ const), therefore the turbulent pressure can be written as

$$p_{\rm t} = 2E_{\rm tot}/3 - E_{\rm m}/3. \tag{2.4}$$

We expect that $E_{\rm m}$ increase as a function of $p_{\rm mag}$, so we can expand it in a series of $p_{\rm mag}$

$$E_{\rm m} = E_{\rm m}(0) + a_T p_{\rm mag} + ..., \tag{2.5}$$

inserting this into equation (2.4) and using expression $q_{\rm p} = a_T/3$, we get

$$p_{\rm t} = p_{\rm t}(0) - q_{\rm p}\frac{\overline{B}^2}{8\pi}. \tag{2.6}$$

The first term is the turbulent pressure in the absence of the large-scale magnetic field, $\overline{B}$, (the net effect of turbulence on the plasma pressure) and the second term determines the turbulent contribution to the mean magnetic pressure. Here, $q_{\rm p}$ is a function of the large-scale magnetic field that is expected to be positive. Thus, the expression for the total pressure gains the form

$$p_{\rm tot} = p_{\rm g} + p_{\rm t}(0) + (1 - q_{\rm p})\frac{\overline{B}^2}{8\pi}. \tag{2.7}$$

We introduce the effective magnetic pressure as

$$P_{\rm eff} = (1 - q_{\rm p})\frac{\overline{B}^2}{8\pi}, \tag{2.8}$$

which can also be written in dimensionless form

$$\mathcal{P}_{\rm eff} = \tfrac{1}{2}(1 - q_{\rm p})\beta^2. \tag{2.9}$$

Here, $\beta = \overline{B}/B_{\rm eq}$, $B_{\rm eq} = \sqrt{4\pi\rho u_{\rm rms}^2}$ is the equipartition value of a magnetic field, where $\rho u_{\rm rms}^2/2$ is the turbulent kinetic energy. One can see from this relation that for $q_{\rm p} > 1$, the effective magnetic pressure is negative, so it decreases the total pressure of the plasma. This gives rise to a large-scale instability (NEMPI) which is driven at the expense of the total turbulence energy.

2.2.2 NEMPI in simulations

In this section I will describe briefly how one can use mean field simulations (MFS) and direct numerical simulations (DNS) to study NEMPI.

In DNS, we solve the equations of magnetohydrodynamics for the velocity $\boldsymbol{U}$, the magnetic vector potential $\boldsymbol{A}$, and the density ρ, and in some cases in the presence of nonvanishing angular velocity $\boldsymbol{\Omega}=\Omega\hat{\boldsymbol{z}}$,

$$\frac{\mathrm{D}\boldsymbol{U}}{\mathrm{D}t} = -c_{\rm s}^2\nabla\ln\rho+\frac{1}{\rho}\boldsymbol{J}\times\boldsymbol{B}-2\boldsymbol{\Omega}\times\rho\boldsymbol{U}+\boldsymbol{f}+\boldsymbol{g}+\boldsymbol{F}_\nu, \tag{2.10}$$

$$\frac{\partial\boldsymbol{A}}{\partial t} = \boldsymbol{U}\times\boldsymbol{B}+\eta\nabla^2\boldsymbol{A}, \tag{2.11}$$

$$\frac{\partial\rho}{\partial t} = -\nabla\cdot\rho\boldsymbol{U}. \tag{2.12}$$

Here, depending on the origin of the initial field, one can use $\boldsymbol{B}=\boldsymbol{B}_0+\nabla\times\boldsymbol{A}$ in the case with imposed initial magnetic field, or $\boldsymbol{B}=\nabla\times\boldsymbol{A}$ for dynamo-generated initial field. $\boldsymbol{B}_0$ is the imposed uniform magnetic field, which can be horizontal or vertical and $\boldsymbol{A}$ is the magnetic vector potential (nonuniform). Viscous force is defined as $\boldsymbol{F}_\nu=\nabla\cdot(2\nu\rho\mathsf{S})$ where ν is kinematic viscosity and S is the traceless rate-of-strain tensor of the flow. $\boldsymbol{J}$ is the current density, and η is magnetic diffusivity. To drive turbulence one has two options, turbulent convection or forced turbulence. In the latter case, a forcing function, $\boldsymbol{f}$, is added to the momentum equation to describe the production of the forced turbulence. This function is a random plane wave changing at every time step with average wavenumber $k_{\rm f}/k_1$. In the case of helical forcing, without an imposed field, helicity activates a dynamo in the form of an α effect.

The averaged momentum equation can be expressed in the form

$$\frac{\partial}{\partial t}\overline{\rho}\,\overline{\boldsymbol{U}}_i=-\frac{\partial}{\partial x_j}\overline{\Pi}_{ij}+\overline{\rho}\,g_i, \tag{2.13}$$

where $\overline{\Pi}_{ij}$ is the averaged momentum stress tensor, which has the form

$$\overline{\Pi}_{ij}=\overline{\Pi}^{\rm m}_{ij}+\overline{\Pi}^{\rm f}_{ij}. \tag{2.14}$$

Here

$$\overline{\Pi}^{\rm m}_{ij}=\overline{\rho}\,\overline{U}_i\overline{U}_j+\delta_{ij}\left(\overline{p}+\tfrac{1}{2}\overline{\boldsymbol{B}}^2\right)-\overline{B}_i\overline{B}_j-2\nu\overline{\rho}\,\overline{\mathsf{S}}_{ij}, \tag{2.15}$$

and

$$\overline{\Pi}^{\rm f}_{ij}=\overline{\rho}\,\overline{u_iu_j}+\tfrac{1}{2}\delta_{ij}\overline{\boldsymbol{b}^2}-\overline{b_ib_j}. \tag{2.16}$$

$\overline{\Pi}^{\rm m}_{ij}$ is the contribution from the mean field and $\overline{\Pi}^{\rm f}_{ij}$ is the contribution from the fluctuating field. As we are interested in the contribution from the fluctuating part that depends on the mean field, we should calculate $\overline{\Pi}^{\rm f}_{ij}$ also for

zero mean field (let us call it $\overline{\Pi}_{ij}^{\rm f0}$), and then subtract it from $\overline{\Pi}_{ij}^{\rm f}$. We can parameterize the dependence of the resulting tensor on the mean magnetic field as $\Delta\overline{\Pi}_{ij}^{\rm f} \equiv \overline{\Pi}_{ij}^{\rm f} - \overline{\Pi}_{ij}^{\rm f0} = -q_{\rm p}\delta_{ij}\overline{\boldsymbol{B}}^2/2 + q_{\rm s}\overline{B}_i\overline{B}_j - q_{\rm g}\overline{g}_i\overline{g}_j$, by introducing coefficients like $q_{\rm p}$, $q_{\rm s}$ and $q_{\rm g}$. Therefore, one challenge related to NEMPI is to calculate these coefficients for different setups. Kemel et al. (2012b) presented a useful parameterization of $q_{\rm p}$ as

$$q_{\rm p} = \frac{q_{\rm p0}}{1+\beta^2/\beta_{\rm p}^2} \equiv \frac{\beta_\star^2}{\beta_{\rm p}^2+\beta^2}, \tag{2.17}$$

where $\beta_\star = \sqrt{q_{\rm p0}}\beta_{\rm p}$. These two parameters, $\beta_\star$ and $\beta_{\rm p}$, are calculated by using direct numerical simulations (DNS).

Here, I also discuss the codes we used to perform our simulations in this thesis; PENCIL CODE (**Papers I**, **II**, **III**, **IV** and **V**) and Nirvana code (**Paper III**). All previous computations concerning NEMPI have been carried out with the PENCIL CODE. This code is an open source code, which was initially developed by Brandenburg and Dobler (2002) and is currently hosted by Github[1]. It uses sixth-order explicit finite differences in space and a third-order accurate time-stepping method. Although the PENCIL CODE proved to be successful in the numerical study of NEMPI and other instabilities, it was also of interest to detect NEMPI using a different code. For this reason, we performed implicit large eddy simulations (ILES) with a finite-volume code, Nirvana[2], which uses a Godunov scheme to solve the equations without including any explicit dissipative coefficients (Ziegler, 2004). This allowed us to investigate the regime of higher Mach numbers without the requirement to adjust the Reynolds number or grid resolution, which can be computationally very heavy and expensive.

In the following, I review studies of NEMPI using MFS and DNS.

2.2.3 Brief history of the past DNS and MFS studies

As mentioned before, the idea of NEMPI first suggested by Kleeorin et al. (1989, 1990), where they derived an expression for the effective magnetic force in the form of

$$\boldsymbol{F}_{\rm m} = -\nabla\left[(1-q_{\rm p})\frac{\overline{\boldsymbol{B}}^2}{8\pi}\right] + \overline{\boldsymbol{B}}\cdot\nabla\left[(1-q_{\rm s})\frac{\overline{\boldsymbol{B}}}{4\pi}\right]. \tag{2.18}$$

Here, $q_{\rm s}$ and $q_{\rm p}$ are nonlinear functions of the large-scale magnetic field, $\overline{\boldsymbol{B}}$, which relate the sum of the Reynolds and Maxwell stresses to the mean magnetic field. Furthermore, the growth rate of NEMPI depends strongly on the large-scale magnetic field.

[1] `http://github.com/pencil-code`

[2] `http://nirvana-code.aip.de/`

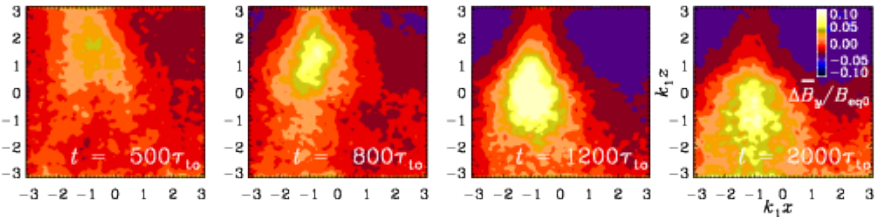

Figure 2.6: First numerical demonstration of NEMPI in DNS that show a large-scale magnetic flux concentration resulting from NEMPI (Brandenburg et al., 2011).

There has been different attempts to derive the functions $q_{\rm p}(\overline{B})$ and $q_{\rm s}(\overline{B})$ by using renormalization approach (Kleeorin and Rogachevskii, 1994) or the spectral τ approach (Kleeorin et al., 1996; Rogachevskii and Kleeorin, 2007). These approaches have been used to take into account the nonlinear terms. Using τ approach one expresses nonlinear terms by a proper damping term, where τ is a damping time. The renormalization approach includes a replacement of real turbulence by the one characterized by effective turbulent transport coefficients. This enables one to derive equations for the transport coefficients –turbulent viscosity, turbulent magnetic diffusivity, and turbulent magnetic coefficients– as a function of scale in the inertial range. The small parameter in the renormalization approach is the ratio of the energy of the mean magnetic field to the turbulent kinetic energy of the background turbulence (with zero-mean fields). Here, it is assumed that the spectrum and statistical properties of the background turbulence are given. Later, Kleeorin and collaborators studied the energy transfer from small-scale to large-scale magnetic field in the case of the negative effective magnetic pressure instability (NEMPI) (Kleeorin et al., 1993, 1996). They suggested NEMPI as a mechanism to explain solar oscillation and sunspot formation. In their model, active regions and sunspots are considered as a shallow phenomenon.

NEMPI was detected in DNS for the first time by Brandenburg et al. (2011). Since then NEMPI become the subject of numerous studies with both DNS and MFS. Figure 2.6 illustrates the formation of a magnetic concentration and its subsequent sinking due to NEMPI. The main reason for sinking is due to the fact that the flux concentration destroys the pressure balance inside and outside of the flux tube, so the gas pressure increases, which leads to the increase of the density. As a result, the structure becomes heavy and sinks. This study has confirmed the result of the similar MFS study, which has been performed earlier by Brandenburg et al. (2010b).

As mentioned before, the functions $q_{\rm p}(\beta)$ and $q_{\rm s}(\beta)$ have been calculated

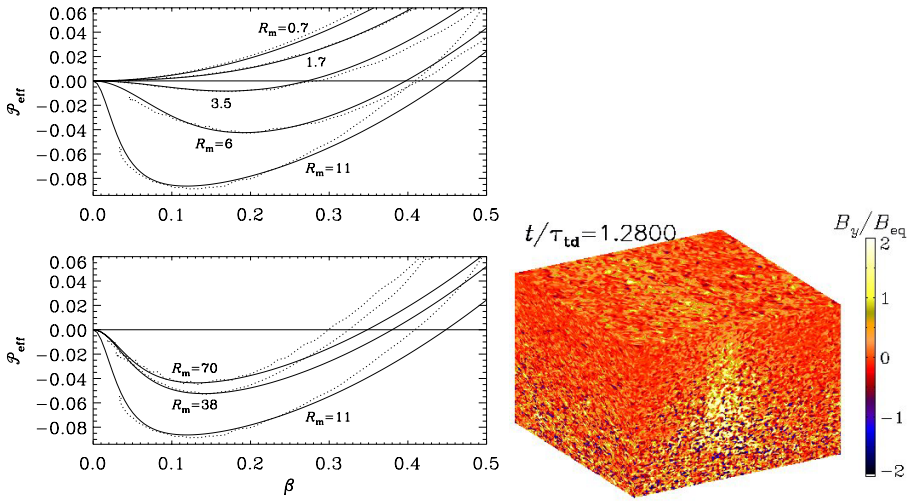

Figure 2.7: Left panel: Normalized effective magnetic pressure versus β for different values of Re_M. Right panel: formation of structures due to NEMPI in 3D simulations (taken from Kemel et al. (2012a)).

analytically by Kleeorin et al. (1990); Rogachevskii and Kleeorin (2007). After detection of NEMPI in DNS, these functions have been determined in the simulations by Brandenburg et al. (2010b, 2012a) and Käpylä et al. (2012). They demonstrated that in a forced turbulence with an imposed weak initial magnetic field, these functions are indeed positive and their value exceeds unity. These results demonstrated how the reduction of the effective Lorentz force occurs, which leads to a negative effective magnetic pressure. According to their simulations, $q_{\rm p}$ should be larger than $2q_{\rm s}$. They also determined the growth rate of this instability and showed that the growth rate increases with increasing $q_{\rm p}$, strength of stratification, and imposed field. They also investigated the effect of magnetic diffusivity and found that increasing the magnetic diffusivity decreases the growth rate. Later, Brandenburg et al. (2012a) clarified that the ratio $B_0/B_{\rm eq0}$ should be in a suitable range to excite NEMPI. The results of these simulations are consistent with theory and mean-field calculations.

Kemel et al. (2012b) investigated NEMPI in MFS in a highly stratified isothermal gas with large plasma β. They demonstrated that NEMPI leads to the formation of three-dimensional structures, which vary along the direction of the imposed initial field (here the y direction). Later, they improved their model to increase the computational domain (to contain higher numbers of turbulent eddies) (Kemel et al., 2012a). The left panel of Figure 2.7 presents

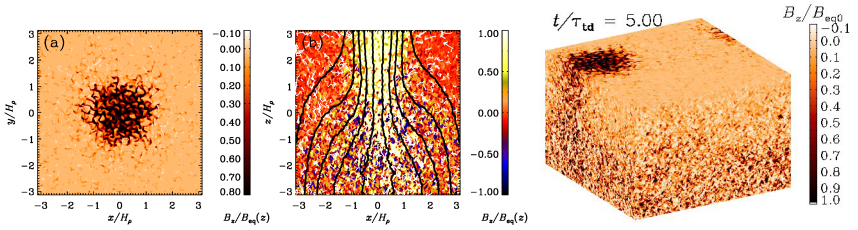

Figure 2.8: Demonstration of NEMPI with vertical imposed field taken from Brandenburg et al. (2013).

normalized effective magnetic pressure versus β for different values of magnetic Reynolds number, Re_M. One can see that for $\mathrm{Re}_M > 3.5$ and $\beta < 0.4$, the effective magnetic pressure is negative, which implies that NEMPI is excited. This leads to the concentration of the magnetic field (see the right panel of Figure 2.7). Kemel et al. (2013b) also studied the effect of non-uniformity of the magnetic field on NEMPI in both MFS and DNS. In this paper, they performed a linear stability analysis to investigate NEMPI. Then, using both MFS and DNS, they considered NEMPI as a possible mechanism for the formation of active regions in the Sun (Kemel et al., 2013a).

All previous studies of NEMPI have been performed in the presence of a forced turbulence. Käpylä et al. (2012) investigated the effects of turbulent convection on NEMPI by including the entropy equation. Their results showed that, NEMPI still works in the presence of an adiabatic background stratification and with convection.

Subsequently, Brandenburg et al. (2013) made an important improvement of the modeling of magnetic field concentration caused by NEMPI. They, for the first time, used a vertical imposed magnetic field with a vertical field boundary condition to excite NEMPI in a forced turbulence of the stratified plasma. In the presence of a vertical imposed field, due to the lack of saturation by what is known as a potato sack effect, the resulting magnetic field is even larger than the equipartition value, and after 1.5 turbulent-diffusive times, it forms a magnetic spot on the surface; see Figure 2.8 both left and right panels. The middle panel of Figure 2.8 presents the vertical cuts through the spot together with the field lines of the numerically averaged mean field.

This achievement motivated us to study NEMPI with a vertical imposed field in more detail. We presented the result of this study in a follow-up paper on this subject (**Paper III**). Because of the importance of this result, I will discuss it in more detail in Chapter 3.

NEMPI was studied also in the presence of rotation using both MFS and DNS by Losada et al. (2012, 2013). They investigated the development of

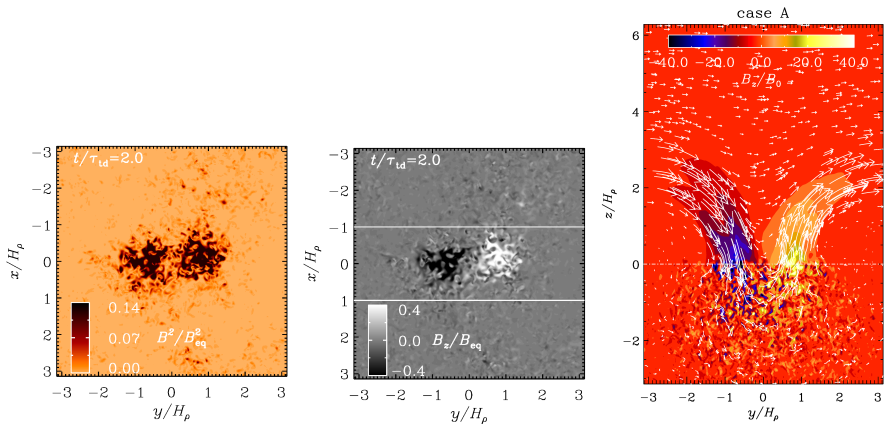

Figure 2.9: Formation of bipolar regions due to NEMPI taken from Warnecke et al. (2013).

NEMPI in the presence of rotation using a large value of the scale separation. Using MFS, they reported that even relatively slow rotation, with Coriolis numbers, $\mathrm{Co} = 2\Omega/u_{\mathrm{rms}}k_{\mathrm{f}}$, around 0.1 suppresses NEMPI. In their next paper, they showed that there is good agreement between DNS and MFS in the case of NEMPI in a rotating system when Co is small. For higher Co, however, the growth rate of NEMPI increases, which was inconsistent with the fact that the rotation suppresses NEMPI (see also Figure 6 of **Paper II**). This implies that there must be another source which provides growth of magnetic field. This mechanism acts at the same time as NEMPI or even after NEMPI was suppressed. One explanation was that for higher values of Co, an α^2 mean-field dynamo is generated and causes this observed growth rate. In other words, for large values of Co we deal with some kind of coupled system of NEMPI and mean-field dynamo. In Chapter 3, I will present the results of a more detailed study of this system, which led to two publications, **Papers I** and **II**. In 2014, Losada et al. (2014) studied NEMPI in a forced turbulence plasma with a non-constant polytropic stratification.

Later, Warnecke et al. (2013, 2016) reported formation of bipolar regions due to NEMPI in DNS. In their simulations, an outer layer with coronal properties (unforced non-turbulent regime) was added to the upper boundary. They demonstrated that the presence of this new upper "boundary condition" helps to the formation of a bipolar magnetic spots (see Figure 2.9).

In the next section, I present different alternatives, which have the potential to be used to explain the formation of sunspots and active regions.

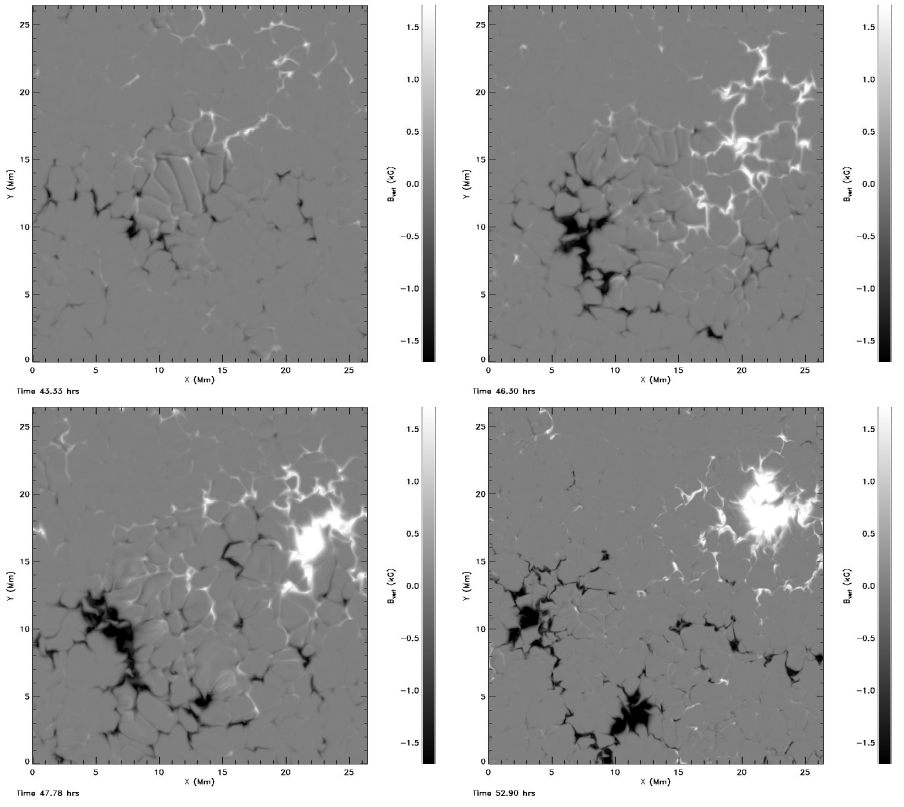

Figure 2.10: Separation of opposite polarity of the magnetic field (magnetic field concentration) on the upper layer due to magnetoconvection taken from Stein and Nordlund (2012).

2.3 Other models

Although the rising flux tube theory was able to explain many observed properties of sunspots and active regions, however, this model has some weaknesses. For instance the flux tubes are expected to expand as they rise, hence their strength weakens and some sort of reamplification mechanism must complement this model to match the observational properties of sunspots. In recent years, there have been several simulation results suggesting possible structure formation near the surface, without assuming a rising flux tube at the bottom of the convection zone (see e.g. Kitchatinov and Mazur, 2000; Brandenburg et al., 2011; Stein and Nordlund, 2012; Mitra et al., 2014; Käpylä et al., 2016) and also **Papers I**, **II**, **III**, **IV**, and **V**.

Employing a mean-field model, Kitchatinov and Mazur (2000) proposed

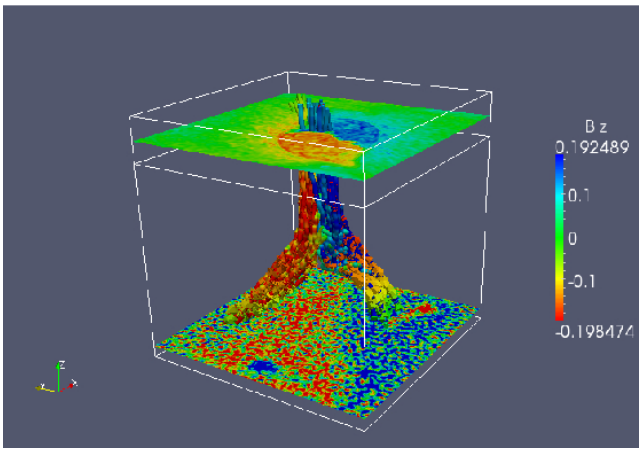

Figure 2.11: Three-dimensional visualization of the vertical magnetic field in simulations of Mitra et al. (2014).

another mechanisms of flux concentrations. they suggested that the suppression of convection motions (heat flux) by a mean magnetic field leads to a decrease in temperature and formation of magnetic field concentration.

Later, Stein and Nordlund (2012) suggested that the interaction of turbulent convection with a shallow uniform horizontal magnetic field leads to the formation of bipolar regions; see Figure 2.10. They showed using a numerical simulation that it is not necessary to have an initially coherent flux tube to form an active region. In particular, magnetoconvection with a horizontal 1 kG magnetic field imposed at the bottom of the computational domain (at a depth of about 20 Mm) gives rise to bipolar structures at the surface and thus leads to the formation of an active region.

Mitra et al. (2014) has shown that in strongly stratified forced two-layer turbulence with helicity and corresponding large-scale dynamo action in the lower layer, and nonhelical turbulence in the upper, a magnetic field concentration occurs in the upper layer in the form of sharply bounded bipolar magnetic spots; see Figure 2.11.

Their results are important, because the strength of the bipolar structures obtained in DNS by Mitra et al. (2014) is about a few times the local equipartition field strength and their origin is related to the underlying dynamo. Other interesting results of Mitra et al. (2014), is the lifetime of the sharp boundary between the bipolar regions, which is longer than what one estimates from the effects of turbulent diffusion. This motivated us to extend this two-layer model to spherical geometry and study it in more detail.

The results of this study in spherical geometry will be discussed in Chap-

ter 4, where I present the results of **Paper IV**. Later, in subsequent paper (**Paper V**), we studied a similar system but in the plane geometry and proposed the magnetic turbulent reconnection as a cause for the long lifetime of bipolar structures. These results will be presented in Chapter 5.

Recently, Käpylä et al. (2016) performed a magnetoconvection simulation similar to that of Stein and Nordlund (2012) with radiation to study the formation of flux concentration in a convective flow. In their model, they investigated stratified turbulent convection in the presence of a weak uniform horizontal and vertical magnetic field in Cartesian domain. They demonstrated that, such a system develops super-equipartition flux concentration near the surface, which grows linearly in time. They also have observed the existence of a converging flow at the location of the spots. They suggested that this converging flow corresponds to the large-scale supergranulation, which is due to convection.

3. Studies of NEMPI

The limits of the possible
can only be defined by going beyond them
into the impossible.

Arthur C. Clarke

Of course it is happening inside your head,
Harry, but why on earth should that
mean it is not real??

Harry Potter and the Deathly Hallows

In this chapter, I will first discuss the motivation for studying NEMPI, then I will present three different setups which I divide into two groups. In the first group, I describe the study of NEMPI in the presence of dynamo-generated magnetic fields and in the second group, I will present the investigation of NEMPI with an imposed vertical magnetic field. I will then present the major results obtain in **Papers I**, **II**, and **III**.

3.1 Motivation

One of the main conditions for the excitation of NEMPI is the presence of an initial weak magnetic field. It has been shown that it must have a field strength in a proper range. However, all previous studies of NEMPI were done using an imposed magnetic field. So one step toward extending this model was to study this instability in the presence of a dynamo-generated magnetic field. Furthermore, we are interested in the investigation of the effect of geometry on NEMPI. In view of application to the Sun, it is important to study NEMPI also in spherical geometry and to study how this instability develops in a spherical shell. I will discuss the result of this study in the next section. Losada et al. (2013) have studied the effect of rotation on NEMPI and have shown that rotation suppresses NEMPI. However, for sufficiently rapid rotation, dynamo action sets in, which leads to a complicated coupled system of dynamo and NEMPI. In order to improve our understanding of this coupled system, we performed a detailed study of this problem which I am going to present in Section 3.2.

As I mentioned before, one of the applications of NEMPI is to explain the formation of active regions and sunspots in the Sun. A typical sunspot has a

field strength of a few times the equipartition field strength. In the studies of NEMPI with imposed horizontal magnetic field, the strength of the resulting field concentration was below the equipartition field value. This problem of a weak resulting field has been overcome by Brandenburg et al. (2013), who for the first time studied the formation of magnetic structures in the presence of a vertical imposed field as initial field. Their simulations showed that it is possible to produce with NEMPI magnetic spots with a field strength close to the equipartition value. This motivated us to investigate NEMPI with a vertical imposed magnetic field. I will describe the result of this study in Section 3.3.

3.2 NEMPI and dynamo-generated magnetic fields

We already described in Chapter 1.1 that one of the ways to create turbulence is to add a forcing function to the momentum equation. It was shown that when the forcing is helical, it leads to the generation of an α^2 dynamo. Furthermore, we discussed that the combination of rotation and strong stratification also produces an alpha effect. In the following I present the results of a mean-field study of NEMPI with a dynamo-generated magnetic field in spherical geometry. Afterwards, I discuss the study of NEMPI focusing on the effect of the combined system of dynamo on NEMPI.

3.2.1 **Paper I**: NEMPI in a spherical geometry

In **Paper I**, we used MFS to study NEMPI with an α^2 dynamo. In particular, we study NEMPI under more realistic conditions like global geometry and dynamo-generated magnetic fields. In a spherical geometry, it is not obvious how one can impose a magnetic field, and it is therefore more straightforward to use a dynamo-generated field. In this study, we investigated the combined effects of a dynamo and NEMPI in a highly stratified turbulent plasma with an adiabatic equation of state. This implies that the stratification is not uniform and varies with depth.

Our simulations showed that it is possible to excite NEMPI when the initial field is dynamo-generated. In fact, these two instabilities, NEMPI and dynamo, work together in a constructive manner. As one expects, when the value of the magnetic field is about a few percent of the equipartition value, NEMPI starts growing. To obtain a suitable saturation magnitude of the mean magnetic field, we used α quenching (this concept was explained in Section 1.3.2).

In Figure 3.1, we compare simulations with different stratifications, where we plotted meridional cross-sections of $B/B_{\rm eq}$ (color coded) together with magnetic field lines of the poloidal magnetic field. Here, $r_\star$ is the stratification parameter and it is defined as the radius outside the star where the tem-

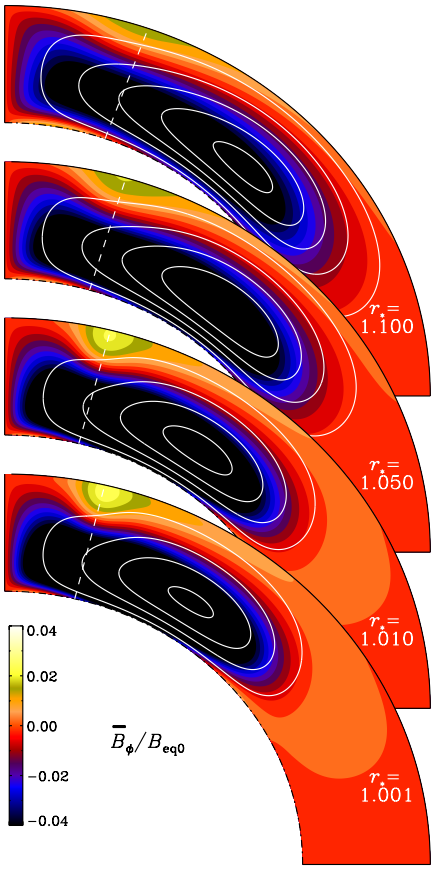

Figure 3.1: The effect of stratification on the development of NEMPI $r_\star$ takes the values 1.100, 1.050, 1.010 and 1.001 (Taken from **Paper I**.)

perature would go to zero. Table 1 of **Paper I** presents the density contrast for different value of $r_\star$. The dashed lines indicate latitudes 49°, 61.5°, 75.6°, and 76.4°. One can see in Figure 3.1 that there are intense field concentrations for stronger stratifications. This is due to the fact that the growth rate of NEMPI is inversely proportional to the density scale height. Therefore, the field concentrations disappear for weaker stratification.

We also studied the effect of quenching on the field concentrations. As I already explained in Section 1.3.2, quenching is an assumption which allows us to control the strength of the saturated magnetic field. Our results showed that for smaller quenching or, in other words, for a stronger mean magnetic field, NEMPI occurs at lower latitudes. Also, for larger quenching, the magnetic field is smaller and NEMPI is more pronounced.

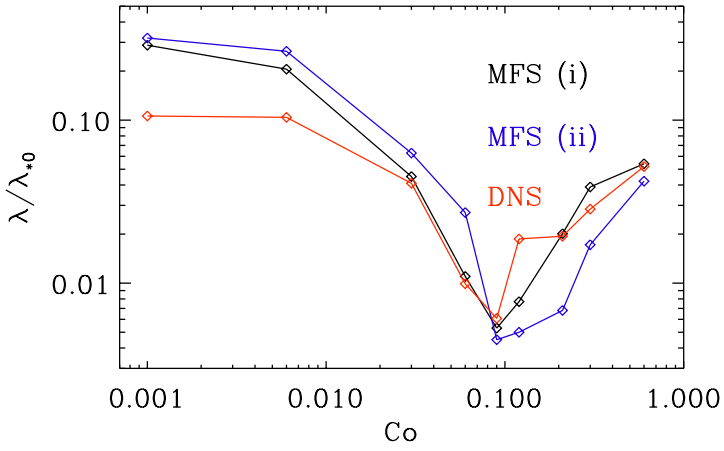

Figure 3.2: Non-dimensional growth rate of NEMPI versus Co for MFS(i) with $\beta_\star = 0.33$ and MFS(ii) with $\beta_\star = 0.44$, as well as DNS for Gr $= 0.033$ and $\beta_0 = 0.05$ (Taken from **Paper II**).

In the case of a very weak initial field, we have found that there is an oscillatory poleward migration, which is due to the effect of NEMPI on the dynamo (see Figures 6 and 7 of the **Paper I**).

3.2.2 **Paper II**: NEMPI and rotation

In the previous section, we showed that by using a dynamo-generated magnetic field to excite NEMPI, one encounters a complicated and combined system of dynamo and NEMPI. Therefore, the main goal of this study is to understand and investigate this coupled system in detail. Here, we adopt a plane geometry and study NEMPI in the presence of rotation using both DNS and MFS.

First, we reproduced the results of Losada et al. (2013) for different rotation rate and measured the growth rate of NEMPI. Figure 3.2 presents the dimensionless growth rate of NEMPI versus the Coriolis number, Co.

One can see that when Co increases the growth rate of NEMPI decreases, which implies that rotation suppresses NEMPI. However, when the Coriolis number increases even further, the growth rate of the instability starts to increase (see Figure 3.2). This implies that due to the high rotation rate (high Coriolis number, Co) and the presence of strong stratification, an α^2 dynamo is excited. In fact, NEMPI works with high stratification, while rapid rotation together with stratification is the key to excite a large-scale dynamo instability. Thus, when we have both NEMPI and rotation in the system, stratification and rotation compete with each other and when the system reaches the dynamo

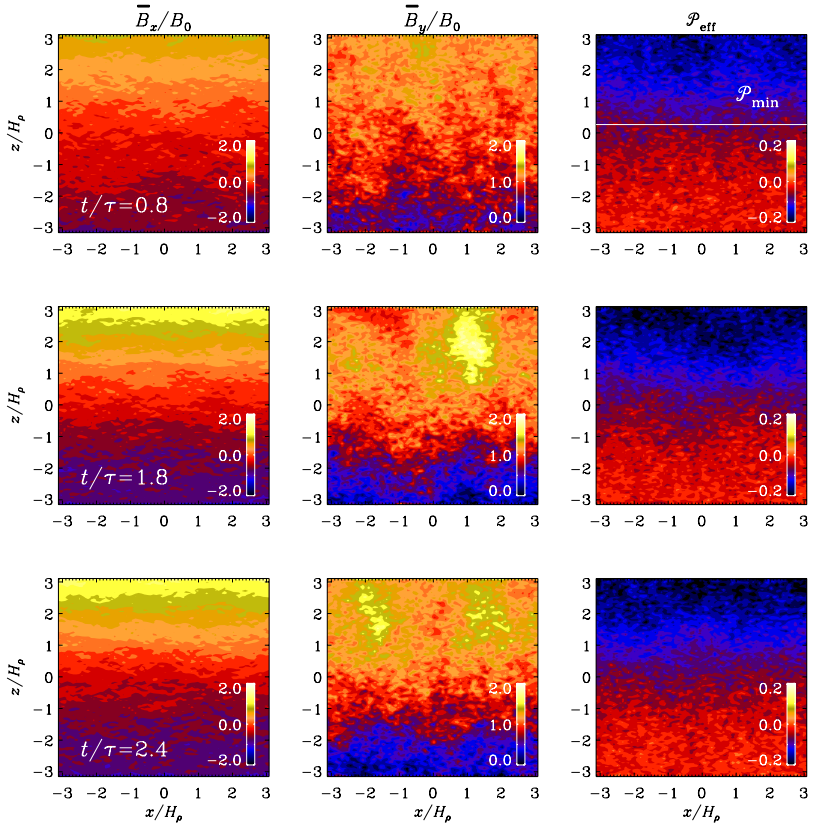

Figure 3.3: Visualization of $\overline{B}_x/B_{\rm eq0}$ and $\overline{B}_y/B_0$ together with effective magnetic pressure for different times. Here $\Omega = 0.15$, Co $= 0.09$, Gr $= 0.033$, and $k_{\rm f}/k_1 = 30$ (Taken from **Paper II**).

threshold, the dynamo instability sets in and creates a large-scale Beltrami-like magnetic field. Figure 3.3 illustrates the x (left column) and y (middle column) components of the resulting magnetic field together with the effective magnetic pressure (right column). As one expects from a Beltrami-like field, the x component has a 90° phase shift relative to the y component of the magnetic field (see Figure 3.3).

We calculated the dynamo number, C_α, using two different approaches. First, we followed the formulation that was presented in Section 1.3.2, and then we performed simulations using test-field method (TFM). Our estimates for the coefficients were close to those calculated using TFM. However, when we compare with earlier works, our coefficients are a bit larger. We believe that these differences are due to the fact that we have used a larger value of

scale separation $k_f = 30$ in our setup (compare with $k_f = 5$ used in previous studies of large-scale dynamos).

Next, we investigated the effects of gravity described by the parameter, $\mathrm{Gr} = g/c_s^2 k_f$, on the growth rate of the instability. We vary Gr by first changing gravity, while the turbulent diffusivity is kept constant and then by varying turbulent diffusivity while g is constant. We observed that our results are independent of the procedure used to change Gr.

Furthermore, we reported that by increasing the stratification, some kind of "gravitational quenching" occurs and the growth rate of the instability decreases again.

3.3 NEMPI and vertical imposed magnetic fields

Brandenburg et al. (2013) showed that by using a weak vertical imposed magnetic field, one can excite NEMPI such that it leads to the formation of magnetic spots with super-equipartition field strength.

We performed both MFS and DNS of highly stratified forced turbulence in an isothermal layer without radiation to study NEMPI in such a system in more detail. In MFS, we adopt a cylindrical coordinates to have the possibility of transforming our problem into an axisymmetric one. In this paper, we investigated the effects of changing the aspect ratio, gravity, Mach number, and scale separation on the formations of magnetic field concentrations. Furthermore, we studied the parameter sensitivity of NEMPI using two different codes, PENCIL CODE and NIRVANA code. As I already mentioned in Section 2.2.2, the NIRVANA code is used for implicit large eddy simulations (ILES). The main advantage of ILES is the lack of physical dissipation coefficients in solving the MHD equations. This gives us the possibility of running simulations with higher Mach numbers without being limited by heavy and expensive simulations due to the high resolution of the setup, which is required for simulations with dissipative terms.

3.3.1 Main results of **Paper III**

The resulting magnetic field has a cellular pattern in our simulations and the number of the cells per unit area is independent of the size of the domain (see Figure 1 of **Paper III**). It was also shown that, the depth where NEMPI occurs varies when the strength of the imposed field changes (Brandenburg et al., 2013). In other word, it increases by increasing the strength of the initial (horizontal or vertical) field. Our MFS results confirmed this statement and showed that the structure moves along the vertical direction when the magnitude of the

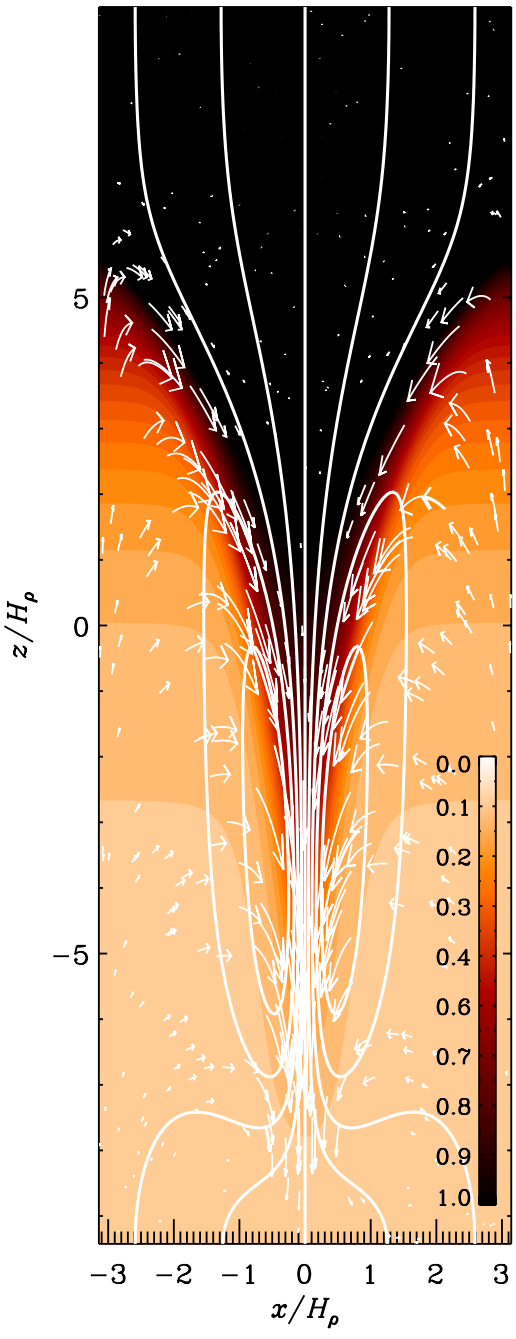

Figure 3.4: $\overline{B}_z/B_{\rm eq}$ together with field lines and flow vectors from MFS. (Taken from **Paper III**.)

imposed field changes. The shape of the flux tube, however, does not change (see Figure 4 of **Paper III**).

We investigated the resulting magnetic field together with velocity vectors at the time of spot formations and reported the existence of an inflow into the flux tube along magnetic field lines at a lower depth. Figure 3.4 presents the vertical component of magnetic field color coded together with magnetic field lines. The white arrows present the velocity vectors. One can see an inflow at a lower depth and an outflow at higher depth. It is this inflow, which keeps the magnetic flux tube concentrated.

We also found that the structure moves upward when we decrease the scale separation. This is because the scale separation is proportional to the inverse turbulent diffusion coefficient. Therefore, by decreasing the scale separation, we increase the diffusivity, which leads to a weaker field concentration. A weaker field concentration sinks less because of horizontal pressure balance. The total pressure balance implies that the sum of the gas pressure and effective magnetic pressure is constant. An increase of the magnetic field increases the gas pressure. For weak magnetic field this increase of the gas pressure is small. Smaller gas pressure leads to smaller density, which implies that the structure becomes lighter and sinks less (see Figure 7 of **Paper III**).

We also studied the effects of rotation on NEMPI in the case with a vertical imposed field. Our results showed that for a vertical imposed field, rotation suppresses NEMPI and, at the same time, the structure moves upward and becomes fatter (see Figure 12 of **Paper III**).

Finally, our simulations with different magnetic Prandtl, Pr_M, and Reynolds numbers, Re_M, demonstrated that for $\mathrm{Pr}_M \geq 8$ and $\mathrm{Re}_M \ll 1$, NEMPI does not work. This is consistent with previous findings. To study the effect of Mach number, we used ILES. We found that for larger Mach number, the magnetic structure becomes smaller, which is due to the fact that the structure forms in the upper layer and cannot be fully contained in our domain.

4. Two-layer model in a spherical shell

Not all those who wander are lost.

J.R.R. Tolkien

In this chapter, I first will discuss the motivation for using a two-layer forcing setup to model the formation of bipolar magnetic structures. I will then describe the main idea and the setup we used and in the last section I will present the major results obtain in **Paper IV**.

4.1 Motivation

As mentioned already in Chapters 2 and 3, a dynamo-generated magnetic field can form magnetic spots due to NEMPI. On the other hand, formation of bipolar structures of super-equipartition field strength and a dynamo-generated initial field, first was reported by Mitra et al. (2014). They performed direct numerical simulations (DNS) of stratified forced turbulence leading to a large-scale α^2 dynamo. In their simulations, the turbulence in the deeper parts was produced to be helical such that a large-scale magnetic field can be generated by the α effect associated with the kinetic helicity of the turbulence. In the upper part of the domain, however, the turbulent forcing was non-helical. They demonstrated that in such a model, intense bipolar structures form at the surface, evolve in time, elongate, move toward each other, interact, and change their form. Later these structures become weak but do not disappear and instead a new structure starts forming again. These structures also have a sharp boundary between opposite polarities. The most surprising result was the fact that these field concentrations have field strengths which exceed the equipartition value by a factor of three or more. Since in their paper, they did not measure the effective magnetic pressure, the mechanism behind the formation of these intense bipolar spots was not obvious. Nevertheless, they reported the existence of a downflows with a strength of about 20% of the turbulent velocity at the location of the spots. This motivated us to study this system in more detail.

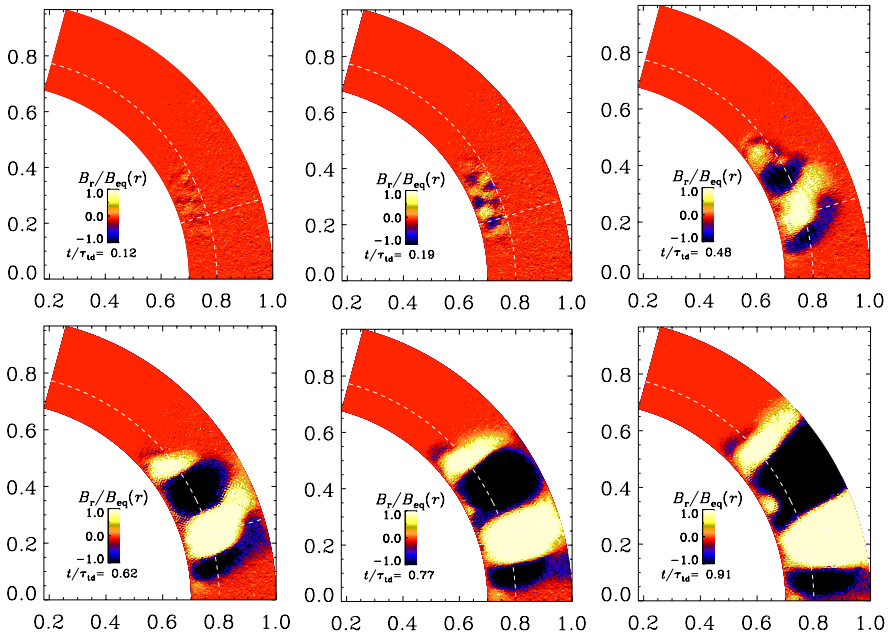

Figure 4.1: Meridional cross-sections of $\overline{B}_r/B_{\rm eq}$ at different times for a simulation with $\Gamma_\rho = 450$ taken from **Paper IV**.

4.2 The setup

One step toward improving this model was to reduce the unwanted effects resulting from the periodic boundary conditions in a plane geometry. When one uses a plane geometry, due to the periodicity in the two horizontal directions, only a single structure forms inside the domain and increasing the size of the domain only leads to the formation of a larger structure. To overcome this artifact we performed the simulations in spherical geometry. This choice had a few advantages; a spherical shell has larger horizontal extent and realistic boundary conditions. In the one hand, this will allow the system to develop more than one structure, which lets us to study also the interaction with neighboring structures. On the other hand, the main purpose of this study is to explain the formation of sunspots and active regions on the solar surface, therefore spherical geometry is an obvious choice to get the opportunity to compare the characteristics of these bipolar structures with what is observed in the Sun.

In **Paper IV**, we study a system similar to that of Mitra et al. (2014), but in spherical geometry. We adopt either symmetric (quadrupolar) or antisymmetric (dipolar) field properties about the equator. Following Mitra et al. (2014), we use an isothermal equation of state, so no convection is possible. In

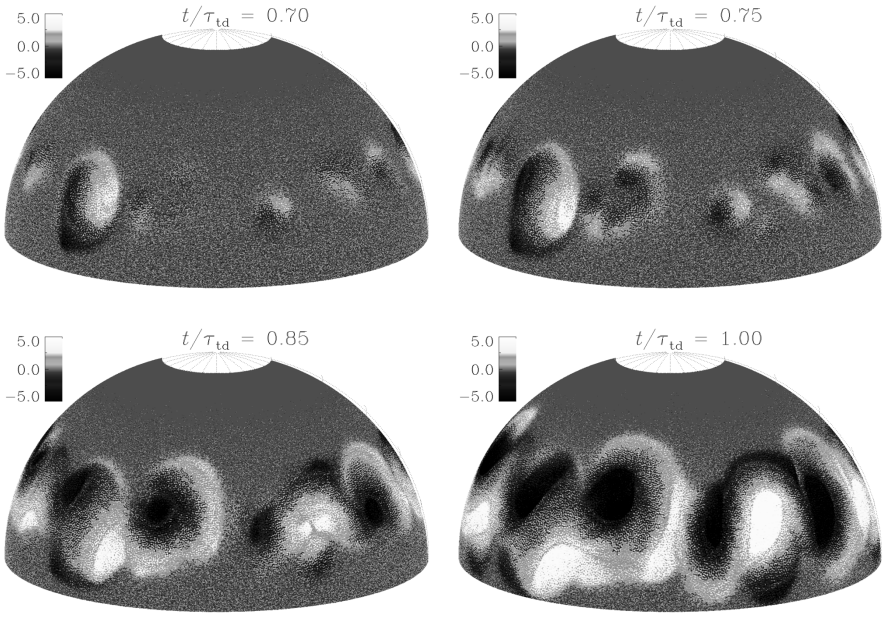

Figure 4.2: Time evolution of $B_r/B_{\rm eq}$ at $r/R = 0.98$ for a simulation with $\Gamma_\rho = 450$ taken from **Paper IV**.

order to create turbulence, we add a non-uniform forcing function to the momentum equation. The forcing profile is chosen to be helical in the lower part of the domain so that the helicity causes the excitation of an alpha squared dynamo. This leads to the generation of a large-scale magnetic field in the lower layer of the spherical shell (see Figure 4.1). In the upper part of the domain, the forcing is non-helical (for more detailed discussion related to the forcing see section 2.2 of **Paper IV**). Figure 4.1 presents the time evolution of $\overline{B}_r/B_{\rm eq}$ on meridional cross-sections. One can see the generation of large-scale magnetic field in the deeper part of the shell, which later propagates toward the surface.

Later, we change the position of the border between these two layers to see how it affects the results. We expect to detect the formation of a similarly intense bipolar region observed in earlier DNS of Mitra et al. (2014). We perform DNS to study the effects of domain size, density stratification, geometry, and boundary conditions on the formation of these bipolar structures.

4.3 Main results of **Paper IV**

We have shown that in a two-layer forcing model in a spherical shell with strong stratification, the α^2 dynamo produces a large-scale magnetic field that

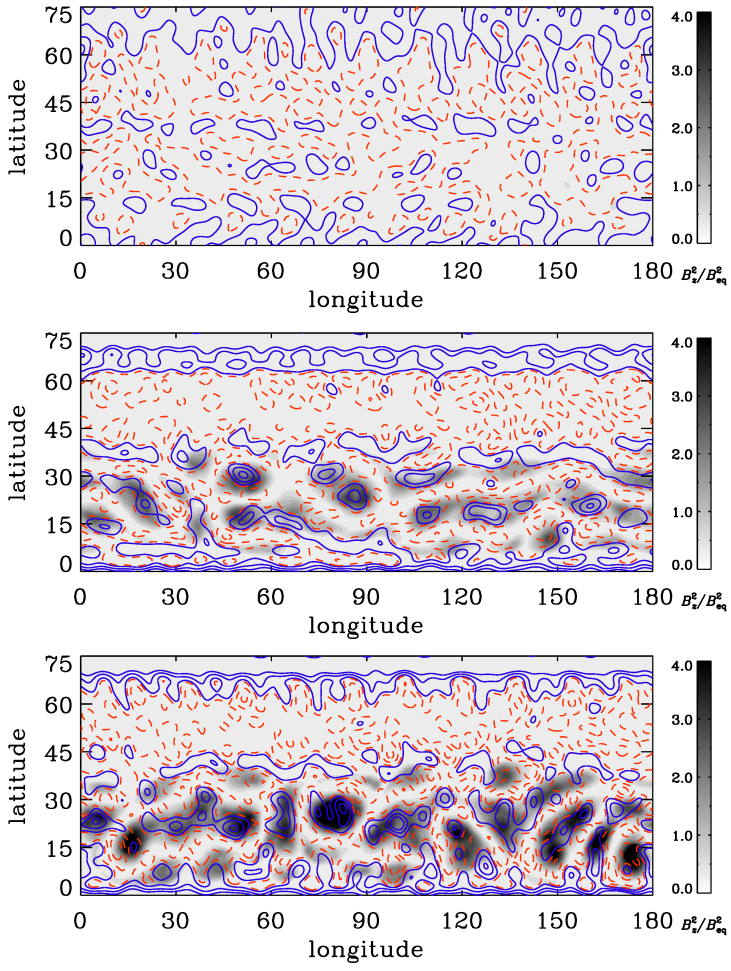

Figure 4.3: Contours of negative (blue, solid lines) and positive (red, dashed) vertical velocity $\langle U_r \rangle_{kR<50}$ superimposed on a gray-scale representation of $\langle B_r \rangle^2_{kR<100}/B^2_{\rm eq}(r)$ in Mercator projection at $r/R = 0.85$ and $t/\tau_{\rm td} = 0.7$ for Runs with different stratifications, $\Gamma_\rho = 2$ (upper panel), $\Gamma_\rho = 450$ (middle panel) and, $\Gamma_\rho = 1400$ (lower panel) taken from **Paper IV**.

later develops into a sharp spot-like bipolar structure at the surface (see Figure 4.2). As one can see in Figure 4.2, these structures expand as time elapses, and eventually fill the entire horizontal surface (see the last panel of Figure 4.2).

We believe that this is due to the strong helicity beneath the surface. Our results for a spherical shell confirm the results of Mitra et al. (2014) in Cartesian geometry, and extend it for a much larger domain. In a spherical shell, for

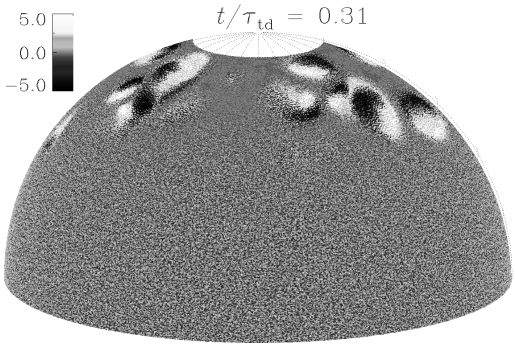

Figure 4.4: Formation of the high-latitude spots for the case $n = 0$ taken from **Paper IV**.

the first time, we observed the formation of bipolar magnetic spots with finite size. However, contrary to earlier studies by Kemel et al. (2012b) and in **Paper III**, the magnetic structures expand and obtain a size larger than the local value of the density scale height. In this study, we found that the dynamo depends on stratification. Stratification also plays a crucial role in the formation of magnetic bipolar structures. In Figure 4.3, where the gray-scale represents $\langle B_r \rangle^2_{kR<100}/B^2_{\rm eq}(r)$, we compare runs for three different stratifications. One can see that for intermediate (middle panel) and strong stratification (lower panel), magnetic spots are formed at the surface. In the upper panel of Figure 4.3, however, due to weak stratification, there is no spots. Furthermore, similar to Mitra et al. (2014), we also detected the downflows in the vicinity of the spots (see the contours of negative (blue, solid lines) vertical velocity, $\langle U_r \rangle_{kR<50}$, in both middle and lower panels of the Figure 4.3).

Since the important role of stratification has been pointed out in the concentration of magnetic field due to NEMPI, it is of interest to measure the effective magnetic pressure in our setup to investigate the possibility of NEMPI in this setup. We found that the effective magnetic pressure is positive near the surface, but it becomes negative in the deeper parts, where the value of the magnetic field strength is still well below the equipartition value.

We also change the helicity profile such that the maximum value of helicity lies near the pole. In such a system, we observe the formation of bipolar spots at high latitudes (see Figure 4.4), similar to what one expects in rapidly rotating cool stars (see Section 2.1.2). The advantage of our model to the previous studies by Yadav et al. (2015) is that in our simulation the spots have both positive and negative polarities.

We also investigated the case, when we changed the location of the bor-

der between two different forcings. We observed that, by moving the border closer to the bottom boundary, the structures appear with a time delay. This is understandable by considering the fact that dynamo waves are the main source of these structures. Therefore, by moving the border to larger depth, it takes longer time for dynamo waves to reach the surface. This scenario is the same when we decrease the amplitude of the helicity.

To compare the obtained magnetic spots with real sunspots we also investigated the orientation of the bipolar structures. These magnetic spots demonstrate a systematic east-west orientation in a way that negative polarity lies on the left and positive one is on the right. Furthermore, some of the regions also possess a certain tilt, although due to existence of the yin-yang structure, it is not easy to determine the sign of this tilt (see Figure 8 of the **Paper IV**).

5. Reconnection of bipolar structures

The true sign of intelligence is not knowledge but imagination.

Albert Einstein

In this chapter, I first describe briefly the main idea and the motivation for the study of the two-layer forcing model, which was already introduced in the previous chapter. Then, I introduce the setup, and in the last section I will present the major results obtained in **Paper V**. In this context, I will emphasize the role of reconnection in the evolution of the bipolar structures.

5.1 Motivation

Our study of a two-layer model in spherical geometry demonstrated that this model has the potential to be used for explaining the formation of bipolar spots. Therefore it is important to investigate this model in detail. Furthermore, it is more straightforward to return to Cartesian geometry where it is possible to study the evolution of a single bipolar spot individually. We already discussed the advantages of using a two-layer model in Section 2.3, and later in Section 4.1, where in the former we discussed the original idea of Mitra et al. (2014) and in the latter, the results of a similar study in spherical geometry were presented (**Paper IV**). To avoid repetition, I just review the key points, which motivated us to perform the research in **Paper V**. The bipolar structures resulting from the two-layer model have a few interesting characteristics. One feature is related to the long lifetime of the spots, which does not obey the traditional picture in MHD, which states that a magnetic concentration decays as time passes due to the effect of turbulent diffusion. This raises the question what sustains the bipolar structure. Therefore, one goal in **Paper V** is to answer this question. Furthermore, the parameter sensitivity of these structures has not been investigated before, so we perform a systematic numerical study to investigate the effects of varying magnetic Reynolds number, scale separation ratio, and Coriolis number. It is beneficial to observe how these structures behave in the presence of rotation.

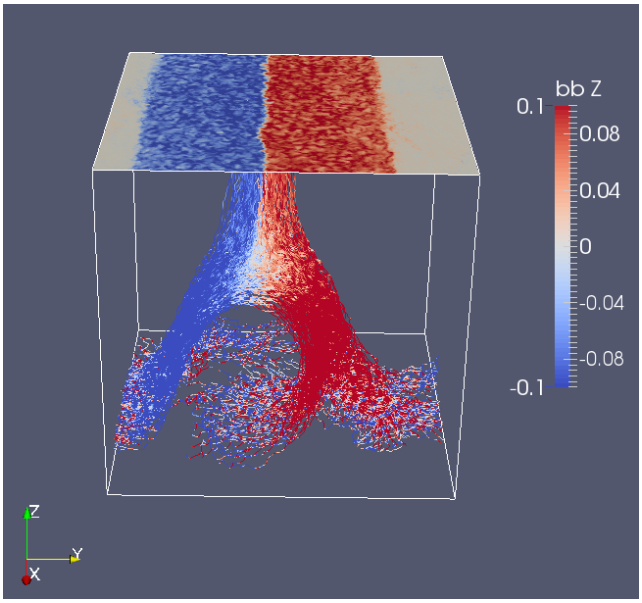

Figure 5.1: Three-dimensional visualization of the vertical magnetic field, B_z, at the surface (color-coded) together with a three-dimensional volume rendering of the vertical component of the magnetic field (Taken from **Paper V**).

5.2 The setup

Our setup is similar to that of Mitra et al. (2014). We perform simulations in a Cartesian domain with size $(2\pi)^3$. The stratification is isothermal with a density contrast of about 535. Turbulence is produced by applying a volume forcing. Following Mitra et al. (2014) and **Paper IV**, the forcing function is defined such that we have helical forcing in the lower part of the domain and non-helical forcing in the upper. This leads to the generation of a large-scale magnetic field in the lower layer due to the α^2 dynamo. For more details regarding the forcing profile, see Mitra et al. (2014) and **Paper V**.

5.3 Main results of **Paper V**

Our simulations show that in two-layer forced turbulence (when helical forcing is at the bottom and non-helical forcing is at the top), intense bipolar spots are formed at the surface. A similar result has been obtained for different values of magnetic Reynolds number, Re_M, and Coriolis number, Co. As expected, the bipolar structures tend to extend over the entire horizontal length of the domain. As a result, only one bipolar structure has been produced, which occa-

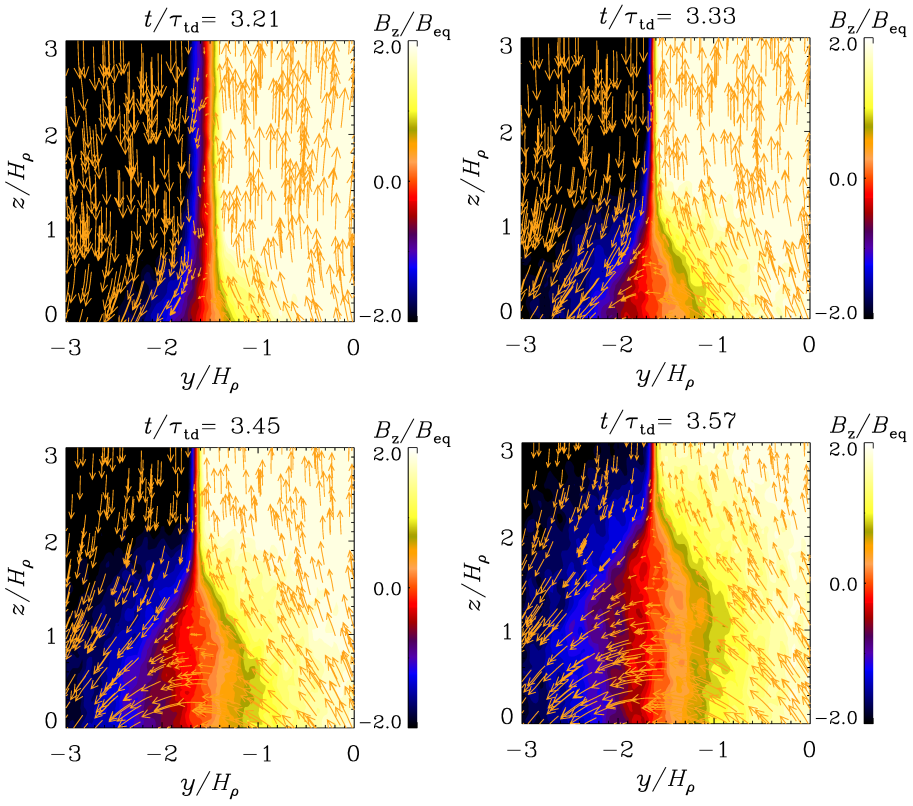

Figure 5.2: Time evolution of $\overline{B}_z/B_{\rm eq}$ together with $(\overline{B}_y, \overline{B}_z)$ vectors (Taken from **Paper V**).

sionally developed band-like structures over the full length of the horizontally periodic domain (see Figure 5.1).

A surprising result in the study of the two-layer model concerns the presence of rotation. As mentioned in Chapter 3, previous studies have shown that even moderate rotation suppresses the magnetic flux concentration in turbulent with an imposed weak magnetic field. Therefore, we expected to see similar behavior here. However, for Co as large as 1.4, the intense bipolar structures still form.

The bipolar structures survive a few turbulent diffusive times. We suggest that the sharp boundary between opposite polarities is constantly being sustained by converging flows. These flows lead to the formation of a current sheet at the interface and eventually the occurrence of turbulent reconnection (see Figure 5.2). Figure 5.2 demonstrates the time evolution of the vertical field, $\overline{B}_z/B_{\rm eq}$, together with vectors of the horizontal field in the yz plane. One

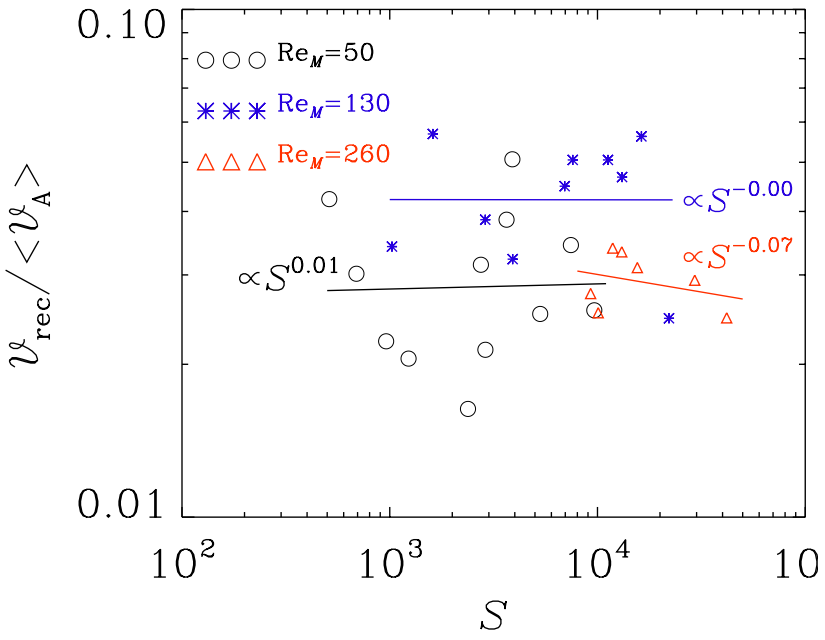

Figure 5.3: Reconnection rate $v_E/\langle v_A \rangle$ (circles) normalized by the mean Alfvén speed versus S. Different panels present different times, entire time interval (upper panel) and time close to the reconnection time (lower panel). The colors represent the value of Re$_M$ (Runs RM1, RM2, and RM3) Taken from **Paper V**.

can see the formation of a current sheet at the sharp interface.

To investigate the reconnection rate in our system, we zoomed in on the area around the boundary between opposite polarities. First, we measured the length of the current sheet to calculate Lundquist number, S. We estimated the reconnection rate using two approaches, which were already explained in Section 1.6. Figure 5.3 presents the result of these calculations, where we have plotted the reconnection rate versus S for different values of Re$_M$.

Our results demonstrate that for high Lundquist numbers, $S > 10^4$, v_{rec} is nearly independent of S, which is in agreement with what one expects from a turbulent regime of reconnection. The measured reconnection rate is also independent of the Alfvén Mach number, M_A^2, as one can see in Figure 5.4.

Furthermore, a comparison was made between the reconnection rate, v_{rec}, resulted from two existing approaches, to show that there is a good agreement between v_{in} and v_E (see Figure 13 of **Paper V**).

We also investigated the flow properties around the bipolar region to compare with previous studies, which have reported the existence of a downflows

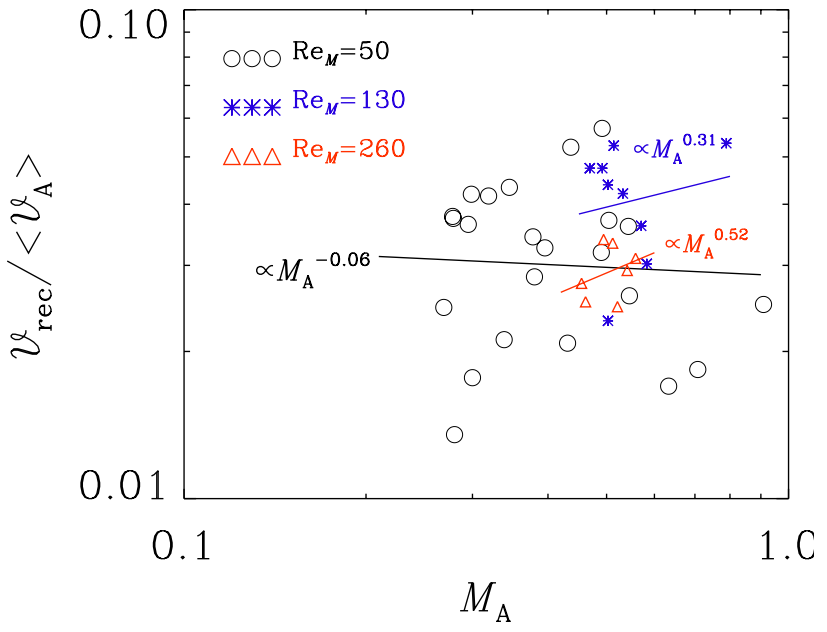

Figure 5.4: The reconnection rate, v_E (circles, solid line) normalized by $\langle v_A \rangle$ as a function of M_A. The solid line presents the best linear fit. Different panels present different values of Re$_M$ (Re$_M$=50 (Run RM1), upper panel, Re$_M$=130 (Run RM2), middle panel, and Re$_M$=260 (Run RM3), lower panel) Taken from **Paper V**.

at the position of the spot. Also in our system, downflows have been detected at the locations of magnetic structure formation (see Figure 7 of **Paper V**).

Finally, we studied the effect of varying the scale separation ratio, k_f/k_1. We decreased k_f/k_1, and observed that, contrary to earlier studies of NEMPI, bipolar magnetic structures are still forming.

6. Outlook

All we have to decide is
what to do with the time that is given to us.

Gandalf the Grey

In this chapter, I would like to give a short overview of unanswered questions regarding the formation of active regions and sunspots. Then, I present possible future improvements of the models studied in my papers.

6.1 Open questions

There are a number of unanswered questions regarding the rising flux tube model, either related to the nature of the dynamo or the origin of sunspots and active regions. There are no certain and complete answers to these questions and there are still many gaps that should be filled either by alternative mechanisms, or with improvements of the flux tube model. One can also think of flux concentrations as a joint result of several mechanisms, which act together at the same time. Here are the main questions:

- Do these flux tubes really physically exist? The picture of a coherent flux tube seems very idealized (Cattaneo et al., 2006).

- How do these flux tubes remain strong and retain their orientation while rising through the turbulent convection zone? The answer to these questions will also address the question "what is their field strength?". It has been shown that the existence of flux tubes with field strengths of 10^5 Gauss are one of the main requirements of the flux transport dynamos (D'Silva and Choudhuri, 1993). This is due to the fact that the flux tube must outcompete the Coriolis force to avoid deflection of its path toward the pole and along the rotation axis during its ascent. It is also necessary to keep the flux tube concentrated while rising through the turbulent convection zone over many scale heights (Choudhuri and Gilman, 1987; Fan et al., 2003). Furthermore, it was shown that such strong magnetic fields are highly unstable (Arlt et al., 2005) and the generation of such field strength has not yet been possible in simulations (Guerrero and Käpylä, 2011). Nelson et al. (2014) performed global convective dynamo simulations to study buoyant magnetic flux tubes. Their results showed that

in such a setup, flux tubes with field strengths of 40 kG are generated due to dynamo action, see also Fan and Fang (2014).

- Is there a collection of magnetic flux tubes that create a sunspot or does each spot result from one single flux tube? This subject is still under debate; see (Rempel and Schlichenmaier, 2011).

- What is the mechanism that re-concentrates the flux tubes near the surface if they have been weakened during the rise? It was suggested by Moreno-Insertis et al. (1995) that a slowly rising flux loop encounters a sudden catastrophic weakening of the field strength (known as explosion of magnetic flux tubes) when it reaches a critical height; see also (Schüssler and Rempel, 2005). There is no direct answer except the ones addressed in the papers corresponding NEMPI or the two-layer model suggested by Mitra et al. (2014).

- How does the buoyancy instability competes against downward pumping? It has been proposed that rising flux tubes due to magnetic buoyancy is the dominant process, although it was shown by Nordlund et al. (1992) that turbulent pumping can compete against the upward motions resulting from magnetic buoyancy.

- How is the magnetic field generated in fully convective stars? In fully convective stars, flux tubes cannot be "stored" anywhere and therefore a different type of dynamo should generate the magnetic field.

6.2 Future improvements

DNS simulations of two-layer models in both Cartesian geometry (**Paper V**) and spherical shells (**Paper IV**) have already demonstrated the possibility of formation of super-equipartition bipolar regions with a dynamo-generated magnetic field. It is therefore of interest to study this model in more detail. For instance, it is important to improve the present two-layer model of **Paper IV** by investigating the effects of rotation, near the surface shear layer, and a real coronal envelope (with a low plasma beta parameter) on the formation of bipolar structures in a spherical shell. One can improve it even further by including differential rotation.

In order to determine the role of NEMPI in the formation of bipolar structures in our two-layer model, it is important to measure the effective magnetic pressure tensors more accurately by developing an adequate test-field method. On the other hand, most previous studies of two-layer models have employed an isothermal equation of state, so another improvement can be to solve the

energy equation by including more physics, e.g., adding a cooling layer at the top, solving the radiative transfer equation in the entire domain, and taking into account ionization. In such models, it may also be possible to detect the turbulent thermo-magnetic instability proposed by Kitchatinov and Mazur (2000). Using convection instead of forced turbulence would be another challenging development in the two-layer model. Furthermore, it would be useful to determine turbulent transport coefficients in both Cartesian and spherical coordinates with dedicated methods such as the test-field approach for our two-layer model to obtain a clear picture of the corresponding dynamo. In many of these developments, it would be more straightforward to study first the system in plane geometry and to understand it better in simplified models.

Recently, we have started investigating the generation of large-scale magnetic fields using a simplified setup in which helicity is driven by the combined effect of stratification and rotation. There, we studied stratified forced turbulence in a Cartesian box, such that the forcing is non-helical in the entire domain. Therefore, to produce helicity, we use the fact that a strong stratification in the presence of rotation is able to produce helicity. Our results have demonstrated that in such a system, helicity is produced which, in the presence of a weak seed magnetic field, leads to the generation of a large-scale magnetic field.

Recent work by Singh et al. (2016) suggested that magnetic flux concentrations affect the surface wave modes and can be detected prior to their appearance on the surface. They used data from the Helioseismic and Magnetic Imager (HMI) aboard the Solar Dynamics Observatory (SDO) and studied the f-mode for three active regions. Their results have demonstrated the strengthening of the f-mode several days before they emerge. By taking into account the fact that a rising flux tube needs just a few hours to reach the surface, the result of Singh et al. (2016) supports the idea of sunspots and active regions being a shallow phenomenon, and that these structures are being assembled gradually over a times pan of days. These results motivate the study of alternative mechanisms of magnetic flux concentrations.

Sammanfattning

Solfläckar och aktiva områden är n ågra av många manifestationer av solens magnetfält. Detta magnetfälts betydelse är väl känd vad gäller uppkomsten av explosiva fenomen såsom koronamassutkastningar (CMEs) och flares men också vad gäller uppvärmningen av solens korona. Därför är det väsentligt att studera solfläckar och aktiva områden och att identifiera de bakomliggande mekanismer som skapar dem. Man tror att så kallade flödesrör (eng. "flux tubes" - rörformade koncentrationer med magnetfält) som flyter upp från botten av konvektionszonen kan förklara uppkomsten av solfläckar, men denna hypotes har inte bekräftats teoretiskt (med numeriska simuleringar) eller med observationer. Ett problem för denna hypotes är att flödesrören förväntas expandera kraftigt när de stiger, vilket betyder att deras magnetfält starkt försvagas. Denna modell behöver därför någon sorts förstärkningsmekanism för att matcha de observerade egenskaperna av solfläckars magnetfält. Om en sådan förstärkningsmekanism inte finns, måste i stället magnetfältet vara mycket starkare där flödesrören skapas i solens inre, än vad som kan förklaras med existerande teorier. Under de senaste åren har det skett en betydande utveckling av en ny modell av magnetfältskoncentrationer med hjälp av den så kallade negativa effektiva magnetiska tryckinstabiliteten (NEMPI) i ett höggradigt skiktat turbulent plasma. Undertryckandet av det totala turbulenstrycket genom ett storskaligt magnetfält leder till en negativ term i det totala medelvärdesbildade trycket. Detta orsakar en storskalig instabilitet. Nyligen har vi för första gången studerat NEMPI i sfärisk geometri och i närvaro av ett dynamogenererat magnetfält. Syftet med dessa studier är att se hur NEMPI växelverkar med ett dynamo-genererad magnetiskt fält. I denna modell är plasmat höggradigt skiktat och en adiabatisk tillståndsekvation tillämpades. Resultaten av medelfälts simuleringar (MFS) visade att NEMPI och dynamomekanismen fungerar mycket bra tillsammans, men också att det resulterande systemet beter sig på ett komplicerat sätt. Detta påvisade att det kopplade systemet av NEMPI och en dynamo behöver studeras i mer detalj. Genom direkta numeriska simuleringar (DNS) visade det sig att redan i närvaro av måttliga Coriolistal ökar tillväxttakten av NEMPI. Detta är inte förenligt med det faktum att rotationen undertrycker NEMPI vilket visade att det måste finnas en annan källa som ger tillväxt. Denna mekanism fungerar samtidigt med NEMPI och även efter det att NEMPI undertryckts. En förklaring – som senare bekräftades av MFS – är att för högre Coriolistal aktiveras en α^2 dynamo vilket orsakar den observerade tillväxttakten. Med andra ord, för stora värden av Coriolistal återfår vi det kända kopplade systemet av NEMPI och dynamo.

I detta sammanhang var det viktigt att kontrollera att dynamo parametern α som vi använder för vår simulering är en korrekt approximation. Av den anledningen har vi också utfört simuleringar med hjälp av testfältmetoden. Det har visat sig att i närvaro av ett vertikalt magnetfält resulterar NEMPI i en magnetfältskoncentration vars fältstyrka är i ekvipartition på grund av ett tillhörande konvergerande plasmaflöde. Detta leder till bildandet av en magnetisk "fläck", som föreslogs vara knuten till flödesröret modellering. Detta motiverade oss att studera fältkoncentrationer som uppkommer med ett vertikalt magnetfält samt egenskaperna hos det resulterande flödesröret. MFS användes för att ta hänsyn till effekten av aspektförhållandet och skalseparationen på NEMPI. Beroendet av magnetfältet, det magnetisk Prandtltalet och det magnetiska Reynoldstalet studerades med DNS. Nyligen har en två-skiktsmodell föreslagits för att studera bildningen av magnetiska strukturer i närvaro av ett dynamo-genererat magnetfält. I denna modell påtvingas turbulensen i hela domänen, men med helicitet enbart i den nedre delen av modellen. Det visade sig att en sådan två-skiktsmodell skulle kunna leda till bildandet av bipolära strukturer med en styrka som motsvarar super-ekvipartition. Detta motiverade oss att studera samma system i sfärisk geometri. Våra resultat visar att när skiktningen är tillräckligt stark bildas intensiva bipolära regioner och med tiden expanderar de, slås ihop och skapar jättestrukturer. Vi studerade två olika helicitetsprofiler och visade att en enkel cosinus profil leder till bildning av fläckar nära polerna, liknande fläckar på en snabbt roterande stjärna. För att förstå den bakomliggande mekanismen för bildandet av sådana intensiva, långlivade bipolära strukturer med en skarp avgränsning, genomförde vi en ny serie av simuleringar i plan geometri och undersökte den här modellen i detalj. Vi genomförde en systematisk numerisk studie genom att variera det magnetiska Reynoldstalet, förhållandet mellan skalseparationen och Coriolistalet. Vi undersökte bildandet av ett flödesskikt mellan bipolära regioner och rekonnektion av magnetiska fältlinjer med motsatt polaritet. Vi bestämde rekonnektionstakten med båda, tillsammans med mätning av inflödeshastigheten i närheten av flödesskiktet och mätning av det elektriska fältet i rekonnektionsregionen. Vi visade att för små Lundquisttal, S <1000, följer rekonnektionstakten Sweet-Parker teorin, men för mycket större S är rekonnektionstakten nästan oberoende av S. Det senare är i överensstämmelse med resultaten av de senaste numeriska simuleringarna, utförda i enklare konfigurationer av andra forskningsgrupper.

Acknowledgments

The tale of love must be heard from love itself.
For like a mirror it is both mute and expressive.

Mevlana jelaluddin rumi

Oh, its quite simple.
If you are a friend, you speak the password,
and the doors will open.

Gandalf

It is time to give my deepest thanks to the people who stood by my side during the last four years of my life and gave me courage to continue. First of all, I dedicate my greatest thanks to my supervisor **Axel**. The person who taught me not only the science, but also the hard work, effort, and enthusiasm. I am very grateful for all the time and effort he gave me over the past few years, for his supports and, guidance, which led me step by step toward the end of my PhD path and the beginning of the research road. I thank him for being very patience whenever I was slow and couldn't catch up with him.

I would like to give many thanks to **Dhruba**, who always had time for my questions, complains, problems, and gave me the best advices I have ever received.

I express my gratitude to my second supervisor, **Göran**, my mentor, **Garrelt**, **Jesper**, the director of graduate studies, and **Göran Östlin**, the head of the department. I should also thank the visitors of our group, **Bengt**, **Matthias**, **Igor** and **Nathan**, whom I learned a lot. I would like to thank all the people in the Astronomy Department and NORDITA for providing such a friendly and warm environment to carry out a very high level of science. A special thanks goes to **Sandra**, **Rocio** and **Hans**, who always were there with a solution to any kind of problems. I want to thank **Jörn**, **Koen**, **Fabio**, and **Simon** for being patient when I was knocking their office door every now and then to ask for help.

I would also acknowledge all the useful conferences (IAU, AGU, SPD, and Pencil-code meetings), including travel grants supported by the American Astronomical Society, the C F Liljevalchs Foundation, the K&A Wallenberg Foundation, the donation scholarship, Alva and Lennart Dahlmark research grant, and the High Performance Computing resources in KTH.

There are also a couple of people, who I would like to thank, especially those who made my PhD studies to be more enjoyable and fun; **Jennifer**, **Nishnat**, **Harsha**, **Xiang-Yu**, **Hiva**, **Saghar**, **Thøger**, **Katia**, **Illa**, **Tine**, **Johan**, **Jayant**, **Johannes**, **Kai Yan**, **Emir**, **Matteo**, **Ruben**, **Alexis**, **Esha**, **Veronica**, **Andrii**, **Maria**, **Carolina**, **Ralf**, **Raffaele**, and **Jino**. I also would like to thank those who already left Stockholm: **Oliver**, **Bidya**, **Barbara**, **Hannes**, **Andreas**, **Florent**, **Atefeh**, and **Nikolas**. I want to give a big thanks to **Jonathan**, a friend who I enjoyed having afternoon tea with and talking about the magical world of books.

Many thanks to **Angelina**, **Giovanni**, **Fabiano**, and **Filippo** for giving me the chance to experience a wonderful traditional Swiss Christmas with real candles on the tree, colorful gifts, and various Swiss dishes. **danke viel mol**.

I want to give a big thanks to **my parents**, my sister **Maria**, my brother, **Amirhossein**, my dearest aunt, **Faranak**, my beloved cousins, **Shadmehr**, **Hamoon**, and **Nima**. I want to thank the whole **Saghatchi** and **Jabbari** families, who supported me all this time from Iran.

Finally, and most importantly, I want to thank **Gianni**. Thank you not just for being there for me whenever I needed you, but also for showing me how to be a strong independent woman. Thank you for wanting to experience new things together and for expanding my horizons. Thank you for teaching me biking, skiing, ice-skating, snorkeling, cooking a perfect rice and introducing me to the delicious Swiss dish, Raclett.

At the end, I am very grateful to know you all, thanks for everything.

May the wind under your wings
bear you where the sun sails
and the moon walks.

Gandalf

References

R. Arlt, A. Sule, and G. Rüdiger. Three-dimensional stability of the solar tachocline. *Astron. Astrophys.*, 441:1171–1175, October 2005. doi: 10.1051/0004-6361:20052928. 55

M. J. Aschwanden. *Physics of the Solar Corona. An Introduction*. Praxis Publishing Ltd, August 2004. 2

A. Beresnyak. On the Rate of Spontaneous Magnetic Reconnection. *ArXiv:1301.7424*, January 2013. 13

E. G. Blackman and A. Brandenburg. Dynamic Nonlinearity in Large-Scale Dynamos with Shear. *Astrophys. J.*, 579:359–373, November 2002. doi: 10.1086/342705. 10

A. Brandenburg. Turbulence and its parameterization in accretion discs. *Astronomische Nachrichten*, 326:787–797, November 2005. doi: 10.1002/asna.200510414. 11

A. Brandenburg and W. Dobler. Hydromagnetic turbulence in computer simulations. *Computer Physics Communications*, 147:471–475, August 2002. doi: 10.1016/S0010-4655(02)00334-X. 26

A. Brandenburg and K. Subramanian. Strong mean field dynamos require supercritical helicity fluxes. *Astron. Nachr.*, 326:400–408, 2005. 6, 8

A. Brandenburg, P. Chatterjee, F. Del Sordo, A. Hubbard, P. J. Käpylä, and M. Rheinhardt. Turbulent transport in hydromagnetic flows. *Physica Scripta Volume T*, 142 (1):014028, December 2010a. doi: 10.1088/0031-8949/2010/T142/014028. 11

A. Brandenburg, N. Kleeorin, and I. Rogachevskii. Large-scale magnetic flux concentrations from turbulent stresses. *Astron. Nachr.*, 331:5, 2010b. 27, 28

A. Brandenburg, K. Kemel, N. Kleeorin, D. Mitra, and I. Rogachevskii. Detection of Negative Effective Magnetic Pressure Instability in Turbulence Simulations. *Astrophys. J. Lett.*, 740:L50, October 2011. doi: 10.1088/2041-8205/740/2/L50. 27, 31

A. Brandenburg, K. Kemel, N. Kleeorin, and I. Rogachevskii. The Negative Effective Magnetic Pressure in Stratified Forced Turbulence. *Astrophys. J.*, 749:179, April 2012a. doi: 10.1088/0004-637X/749/2/179. 11, 28

A. Brandenburg, K.-H. Rädler, and K. Kemel. Mean-field transport in stratified and/or rotating turbulence. *Astron. Astrophys.*, 539:A35, March 2012b. doi: 10.1051/0004-6361/201117871. 10

A. Brandenburg, N. Kleeorin, and I. Rogachevskii. Self-assembly of Shallow Magnetic Spots through Strongly Stratified Turbulence. *Astrophys. J. Lett.*, 776:L23, October 2013. doi: 10.1088/2041-8205/776/2/L23. 29, 36, 40

A. S. Brun, M. S. Miesch, and J. Toomre. Global-Scale Turbulent Convection and Magnetic Dynamo Action in the Solar Envelope. *Astrophys. J.*, 614:1073–1098, October 2004. doi: 10.1086/423835. 19

S. Candelaresi and A. Brandenburg. Kinetic helicity needed to drive large-scale dynamos. *Phys. Rev. E*, 87(4):043104, April 2013. doi: 10.1103/PhysRevE.87.043104. 10

M. Carlsson, J. Leenaarts, and B. De Pontieu. What Do IRIS Observations of Mg II k Tell Us about the Solar Plage Chromosphere? *Astrophys. J. Lett.*, 809:L30, August 2015. doi: 10.1088/2041-8205/809/2/L30. 2

F. Cattaneo, N. H. Brummell, and K. S. Cline. What is a flux tube? On the magnetic field topology of buoyant flux structures. *Month. Not. Roy. Astron. Soc.*, 365:727–734, January 2006. doi: 10.1111/j.1365-2966.2005.09741.x. 55

P. Chatterjee, V. Hansteen, and M. Carlsson. Modeling Repeatedly Flaring δ Sunspots. *ArXiv:1601.00749*, January 2016. 14, 21

M. C. M. Cheung, M. Schüssler, T. D. Tarbell, and A. M. Title. Solar Surface Emerging Flux Regions: A Comparative Study of Radiative MHD Modeling and Hinode SOT Observations. *Astrophys. J.*, 687:1373–1387, November 2008. doi: 10.1086/591245. 21

M. C. M. Cheung, M. Rempel, A. M. Title, and M. Schüssler. Simulation of the Formation of a Solar Active Region. *Astrophys. J.*, 720:233–244, September 2010. doi: 10.1088/0004-637X/720/1/233. 21

A. R. Choudhuri and P. A. Gilman. The influence of the Coriolis force on flux tubes rising through the solar convection zone. *Astrophys. J.*, 316:788–800, 1987. 55

J. Christensen-Dalsgaard. Lecture notes on stellar oscillations. 2003. 16

T.C. Clune, J.R. Elliott, M.S. Miesch, J. Toomre, and G.A. Glatzmaier. Computational aspects of a code to study rotating turbulent convection in spherical shells. *Parallel Computing*, 25(4):361 – 380, 1999. ISSN 0167-8191. doi: http://dx.doi.org/10.1016/S0167-8191(99)00009-5. URL `http://www.sciencedirect.com/science/article/pii/S0167819199000095`. 19

J. de la Cruz Rodríguez, D. Kiselman, and M. Carlsson. Solar velocity references from 3D HD photospheric models. *Astron. Astrophys.*, 528:A113, April 2011. doi: 10.1051/0004-6361/201015664. 2

S. D'Silva and A. R. Choudhuri. A theoretical model for tilts of bipolar magnetic regions. *Astron. Astrophys.*, 272:621, May 1993. 19, 55

Y. Fan. Magnetic fields in the solar convection zone. *Living Reviews in Solar Physics*, 6:4, 2009. 19

Y. Fan and F. Fang. A Simulation of Convective Dynamo in the Solar Convective Envelope: Maintenance of the Solar-like Differential Rotation and Emerging Flux. *Astrophys. J.*, 789:35, July 2014. doi: 10.1088/0004-637X/789/1/35. 56

Y. Fan, W. P. Abbett, and G. H. Fisher. The dynamic evolution of twisted magnetic flux tubes in a three-dimensional convecting flow. I. Uniformly buoyant horizontal tubes. *Astrophys. J.*, 582:1206–1219, 2003. 55

M. Gaurat, L. Jouve, F. Lignières, and T. Gastine. Evolution of a magnetic field in a differentially rotating radiative zone. *Astron. Astrophys.*, 580:A103, August 2015. doi: 10.1051/0004-6361/201526125. 7

A. V. Getling, R. Ishikawa, and A. A. Buchnev. Development of Active Regions: Flows, Magnetic-Field Patterns and Bordering Effect. *Sol. Phys.*, January 2016. doi: 10.1007/s11207-015-0844-3. 15

L. Gizon, A. C. Birch, and H. C. Spruit. Local Helioseismology: Three-Dimensional Imaging of the Solar Interior. *Ann. Rev. Astron. Astrophys.*, 48:289–338, September 2010. doi: 10.1146/annurev-astro-082708-101722. 16

T. P. Golding, J. Leenaarts, and M. Carlsson. Non-equilibrium Helium Ionization in an MHD Simulation of the Solar Atmosphere. *Astrophys. J.*, 817:125, February 2016. doi: 10.3847/0004-637X/817/2/125. 2

A. Greco, S. Perri, S. Servidio, E. Yordanova, and P. Veltri. The Complex Structure of Magnetic Field Discontinuities in the Turbulent Solar Wind. *ArXiv:1511.03084*, November 2015. 3

G. Guerrero and P. J. Käpylä. Dynamo action and magnetic buoyancy in convection simulations with vertical shear. *Astron. Astrophys.*, 533:A40, 2011. 19, 20, 21, 55

G. E. Hale. On the probable existence of a magnetic field in sun-spots. *Astrophys. J.*, 28:315, 1908. 4

V. M. J. Henriques and D. Kiselman. Ca II H sunspot tomography from the photosphere to the chromosphere. *Astron. Astrophys.*, 557:A5, September 2013. doi: 10.1051/0004-6361/201321656. 2

Y. M. Huang and A. Bhattacharjee. Scaling laws of resistive magnetohydrodynamic reconnection in the high-Lundquist-number, plasmoid-unstable regime. *Physics of Plasmas*, 17(6):062104–062104, June 2010. doi: 10.1063/1.3420208. 13

S. Ilonidis, J. Zhao, and A. Kosovichev. Detection of Emerging Sunspot Regions in the Solar Interior. *Science*, 333:993, August 2011. doi: 10.1126/science.1206253. 15

S. Jabbari. Origin of solar surface activity and sunspots. *Licentiate Thesis*, 2014b. 11, 23

L. Jouve and A. S. Brun. 3-D non-linear evolution of a magnetic flux tube in a spherical shell: The isentropic case. *Astronomische Nachrichten*, 328:1104, December 2007. doi: 10.1002/asna.200710887. 17, 19

L. Jouve and A. S. Brun. Three-Dimensional Nonlinear Evolution of a Magnetic Flux Tube in a Spherical Shell: Influence of Turbulent Convection and Associated Mean Flows. *Astrophys. J.*, 701:1300–1322, August 2009. doi: 10.1088/0004-637X/701/2/1300. 18, 19

L. Jouve, B. P. Brown, and A. S. Brun. Exploring the P_{cyc} vs. P_{rot} relation with flux transport dynamo models of solar-like stars. *Astron. Astrophys.*, 509:A32, January 2010a. doi: 10.1051/0004-6361/200913103. 19

L. Jouve, M. R. E. Proctor, and G. Lesur. Buoyancy-induced time delays in Babcock-Leighton flux-transport dynamo models. *Astron. Astrophys.*, 519:A68, September 2010b. doi: 10.1051/0004-6361/201014455. 19

L. Jouve, A. S. Brun, and G. Aulanier. Global dynamics of subsurface solar active regions. *Astrophys. J.*, 762:4, January 2013. doi: 10.1088/0004-637X/762/1/4. 19, 20, 21

L. Jouve, T. Gastine, and F. Lignières. Three-dimensional evolution of magnetic fields in a differentially rotating stellar radiative zone. *Astron. Astrophys.*, 575:A106, March 2015. doi: 10.1051/0004-6361/201425240. 6

P. J. Käpylä, A. Brandenburg, N. Kleeorin, M. J. Mantere, and I. Rogachevskii. Negative effective magnetic pressure in turbulent convection. *Month. Not. Roy. Astron. Soc.*, 422:2465–2473, 2012. 11, 28, 29

P. J. Käpylä, A. Brandenburg, N. Kleeorin, M. J. Käpylä, and I. Rogachevskii. Magnetic flux concentrations from turbulent stratified convection. *ArXiv:1511.03718*, February 2016. 31, 33

K. Kemel, A. Brandenburg, N. Kleeorin, D. Mitra, and I. Rogachevskii. Spontaneous Formation of Magnetic Flux Concentrations in Stratified Turbulence. *Sol. Phys.*, 280:321–333, October 2012a. doi: 10.1007/s11207-012-9949-0. 28

K. Kemel, A. Brandenburg, N. Kleeorin, and I. Rogachevskii. Properties of the negative effective magnetic pressure instability. *Astron. Nachr.*, 333:95, February 2012b. doi: 10.1002/asna.201111638. 26, 28, 47

K. Kemel, A. Brandenburg, N. Kleeorin, D. Mitra, and I. Rogachevskii. Active Region Formation through the Negative Effective Magnetic Pressure Instability. *Sol. Phys.*, 287:293–313, October 2013a. doi: 10.1007/s11207-012-0031-8. 29

K. Kemel, A. Brandenburg, N. Kleeorin, and I. Rogachevskii. Non-uniformity effects in the negative effective magnetic pressure instability. *Physica Scripta Volume T*, 155(1):014027, July 2013b. doi: 10.1088/0031-8949/2013/T155/014027. 29

D. Kiselman. NLTE effects on oxygen lines. *New Astron. Rev.,*, 45:559–563, July 2001. doi: 10.1016/S1387-6473(01)00127-0. 2

D. Kiselman. Solar 3D models versus observations — a few comments. *Physica Scripta Volume T*, 133(1):014016, December 2008. doi: 10.1088/0031-8949/2008/T133/014016. 2

D. Kiselman, T. M. D. Pereira, B. Gustafsson, M. Asplund, J. Meléndez, and K. Langhans. Is the solar spectrum latitude-dependent?. An investigation with SST/TRIPPEL. *Astron. Astrophys.*, 535:A14, November 2011. doi: 10.1051/0004-6361/201117553. 2

L. L. Kitchatinov and M. V. Mazur. Stability and equilibrium of emerged magnetic flux. *Sol. Phys.*, 191:325–340, 2000. 31, 57

N. Kleeorin and I. Rogachevskii. Effective Ampère force in developed magnetohydrodynamic turbulence. *Phys. Rev. E*, 50:2716–2730, 1994. 27

N. Kleeorin, I. Rogachevskii, and A. Ruzmaikin. Magnetic force reversal and instability in a plasma with developed magnetohydrodynamic turbulence. *Sov. Phys. JETP*, 70:878–883, 1990. 11, 23, 24, 26, 28

N. Kleeorin, M. Mond, and I. Rogachevskii. Magnetohydrodynamic instabilities in developed small-scale turbulence. *Phys. Fluids B*, 5:4128–4134, 1993. 27

N. Kleeorin, M. Mond, and I. Rogachevskii. Magnetohydrodynamic turbulence in solar convective zone as a source of oscillations and sunspot formation. *Astron. Astrophys.*, 307:293–309, 1996. 23, 27

N. I. Kleeorin, I. V. Rogachevskii, and A. A. Ruzmaikin. The effect of negative magnetic pressure and the large-scale magnetic field instability in the solar convective zone. *Pisma Astron. Zh.*, 15:639–645, 1989. 23, 24, 26

J. A. Klimchuk. Key aspects of coronal heating. *Philosophical Transactions of the Royal Society of London Series A*, 373:20140256–20140256, April 2015. doi: 10.1098/rsta.2014.0256. 3

O. Kochukhov and N. Piskunov. Doppler Imaging of stellar magnetic fields. II. Numerical experiments. *Astron. Astrophys.*, 388:868–888, June 2002. doi: 10.1051/0004-6361:20020300. 15

O. Kochukhov, N. Piskunov, I. Ilyin, S. Ilyina, and I. Tuominen. Doppler Imaging of stellar magnetic fields. III. Abundance distribution and magnetic field geometry of alpha ^{2} CVn. *Astron. Astrophys.*, 389:420–438, July 2002. doi: 10.1051/0004-6361:20020299. 15

O. Kochukhov, N. Piskunov, M. Sachkov, and D. Kudryavtsev. Inhomogeneous distribution of mercury on the surfaces of rapidly rotating HgMn stars. *Astron. Astrophys.*, 439:1093–1098, September 2005. doi: 10.1051/0004-6361:20053123. 22

G. Kowal, A. Lazarian, E. T. Vishniac, and K. Otmianowska-Mazur. Numerical Tests of Fast Reconnection in Weakly Stochastic Magnetic Fields. *Astrophys. J.*, 700: 63–85, July 2009. doi: 10.1088/0004-637X/700/1/63. 12, 13

F. Krause and K.-H. Rädler. *Mean-field magnetohydrodynamics and dynamo theory*. Pergamon Press, Ltd., Oxford, 1980. 9

A. Lazarian and E. T. Vishniac. Reconnection in a Weakly Stochastic Field. *Astrophys. J.*, 517:700–718, June 1999. doi: 10.1086/307233. 13

J. Leenaarts, M. Carlsson, and L. Rouppe van der Voort. On Fibrils and Field Lines: the Nature of Hα Fibrils in the Solar Chromosphere. *Astrophys. J.*, 802:136, April 2015. doi: 10.1088/0004-637X/802/2/136. 2

I. R. Losada, A. Brandenburg, N. Kleeorin, D. Mitra, and I. Rogachevskii. Rotational effects on the negative magnetic pressure instability (Paper I). *Astron. Astrophys.*, 548:A49, December 2012. doi: 10.1051/0004-6361/201220078. 29

I. R. Losada, A. Brandenburg, N. Kleeorin, and I. Rogachevskii. Competition of rotation and stratification in flux concentrations. *Astron. Astrophys.*, 556:A83, August 2013. doi: 10.1051/0004-6361/201220939. 10, 29, 35, 38

I. R. Losada, A. Brandenburg, N. Kleeorin, and I. Rogachevskii. Magnetic flux concentrations in a polytropic atmosphere (Paper III). *Astron. Astrophys.*, 564:A2, April 2014. doi: 10.1051/0004-6361/201322315. 30

N. F. Loureiro, D. A. Uzdensky, A. A. Schekochihin, S. C. Cowley, and T. A. Yousef. Turbulent magnetic reconnection in two dimensions. *Month. Not. Roy. Astron. Soc.*, 399:L146–L150, October 2009. doi: 10.1111/j.1745-3933.2009.00742.x. 13

N. F. Loureiro, R. Samtaney, A. A. Schekochihin, and D. A. Uzdensky. Magnetic reconnection and stochastic plasmoid chains in high-Lundquist-number plasmas. *Physics of Plasmas*, 19(4):042303–042303, April 2012. doi: 10.1063/1.3703318. 13

L. Mestel. *Stellar magnetism*. 1999. 5

M. S. Miesch, J. R. Elliott, J. Toomre, T. L. Clune, G. A. Glatzmaier, and P. A. Gilman. Three-dimensional Spherical Simulations of Solar Convection. I. Differential Rotation and Pattern Evolution Achieved with Laminar and Turbulent States. *Astrophys. J.*, 532:593–615, March 2000. doi: 10.1086/308555. 19

D. Mitra, A. Brandenburg, N. Kleeorin, and I. Rogachevskii. Intense bipolar structures from stratified helical dynamos. *Month. Not. Roy. Astron. Soc.*, 445:761–769, November 2014. doi: 10.1093/mnras/stu1755. 31, 32, 43, 44, 45, 46, 47, 49, 50, 56

H. K. Moffatt. *Magnetic field generation in electrically conducting fluids*. Cambridge University Press, 1978. 9

F. Moreno-Insertis, P. Caligari, and M. Schuessler. "Explosion" and Intensification of Magnetic Flux Tubes. *Astrophys. J.*, 452:894, October 1995. doi: 10.1086/176357. 56

N. J. Nelson, B. P. Brown, A. Sacha Brun, M. S. Miesch, and J. Toomre. Buoyant Magnetic Loops Generated by Global Convective Dynamo Action. *Sol. Phys.*, 289: 441–458, February 2014. doi: 10.1007/s11207-012-0221-4. 55

Å. Nordlund, A. Brandenburg, R. L. Jennings, M. Rieutord, J. Ruokolainen, R. F. Stein, and I. Tuominen. Dynamo action in stratified convection with overshoot. *Astrophys. J.*, 392:647–652, 1992. 56

J. S. Oishi, M.-M. Mac Low, D. C. Collins, and M. Tamura. Self-generated Turbulence in Magnetic Reconnection. *Astrophys. J. Lett.*, 806:L12, June 2015. doi: 10.1088/2041-8205/806/1/L12. 13

E. N. Parker. The formation of sunspots from the solar toroidal field. *Astrophys. J.*, 121:491, 1955a. 17

E. N. Parker. Hydromagnetic Dynamo Models. *Astrophys. J.*, 122:293, September 1955b. doi: 10.1086/146087. 7

E. N. Parker. Sweet's Mechanism for Merging Magnetic Fields in Conducting Fluids. *J. of Geophysical Research*, 62:509–520, December 1957. doi: 10.1029/JZ062i004p00509. 12

E. N. Parker. Sunspots and the physics of magnetic flux tubes. I - The general nature of the sunspot. II - Aerodynamic drag. *Astrophys. J.*, 230:905–923, 1979. 17, 18

S. Perri, E. Yordanova, V. Carbone, P. Veltri, L. Sorriso-Valvo, R. Bruno, and M. André. Magnetic turbulence in space plasmas: Scale-dependent effects of anisotropy. *Journal of Geophysical Research (Space Physics)*, 114:A02102, February 2009. doi: 10.1029/2008JA013491. 3

N. Piskunov and O. Kochukhov. Doppler Imaging of stellar magnetic fields. I. Techniques. *Astron. Astrophys.*, 381:736–756, January 2002. doi: 10.1051/0004-6361:20011517. 15

M. Rempel. Numerical Sunspot Models: Robustness of Photospheric Velocity and Magnetic Field Structure. *Astrophys. J.*, 750:62, May 2012. doi: 10.1088/0004-637X/750/1/62. 21

M. Rempel and M. C. M. Cheung. Numerical Simulations of Active Region Scale Flux Emergence: From Spot Formation to Decay. *Astrophys. J.*, 785:90, April 2014. doi: 10.1088/0004-637X/785/2/90. 21, 22

M. Rempel and R. Schlichenmaier. Sunspot Modeling: From Simplified Models to Radiative MHD Simulations. *Living Reviews in Solar Physics*, 8, September 2011. doi: 10.12942/lrsp-2011-3. 21, 56

M. Rempel, M. Schüssler, and M. Knölker. Radiative Magnetohydrodynamic Simulation of Sunspot Structure. *Astrophys. J.*, 691:640–649, January 2009. doi: 10.1088/0004-637X/691/1/640. 21

I. Rogachevskii and N. Kleeorin. Magnetic fluctuations and formation of large-scale inhomogeneous magnetic structures in a turbulent convection. *Phys. Rev. E*, 76(5): 056307, 2007. 27, 28

A. Schad, L. Jouve, T. L. Duvall, M. Roth, and S. Vorontsov. Recent Developments in Helioseismic Analysis Methods and Solar Data Assimilation. *Space Science Rev.,*, 196:221–249, December 2015. doi: 10.1007/s11214-015-0199-y. 15

G. B. Scharmer, V. M. J. Henriques, D. Kiselman, and J. de la Cruz Rodríguez. Detection of Convective Downflows in a Sunspot Penumbra. *Science*, 333:316, July 2011. doi: 10.1126/science.1206429. 4

M. Schrinner, K.-H. Rädler, D. Schmitt, M. Rheinhardt, and U. Christensen. Mean-field view on rotating magnetoconvection and a geodynamo model. *Astronomische Nachrichten*, 326:245–249, April 2005. doi: 10.1002/asna.200410384. 11

M. Schrinner, K.-H. Rädler, D. Schmitt, M. Rheinhardt, and U. R. Christensen. Mean-field concept and direct numerical simulations of rotating magnetoconvection and the geodynamo. *Geophysical and Astrophysical Fluid Dynamics*, 101:81–116, April 2007. doi: 10.1080/03091920701345707. 11

M. Schuessler and S. K. Solanki. Why rapid rotators have polar spots. *Astron. Astrophys.*, 264:L13–L16, 1992. 22

M. Schüssler and M. Rempel. The dynamical disconnection of sunspots from their magnetic roots. *Astron. Astrophys.*, 441:337–346, October 2005. doi: 10.1051/0004-6361:20052962. 56

N. Singh, H. Raichur, and A. Brandenburg. High-wavenumber solar f-mode strengthening prior to active region formation. *ApJL.*, January 2016. 15, 57

S. K. Solanki. Sunspots: an overview. *Astron. Astrophys. Rep.*, 11:153–286, 2003. 4

H. C. Spruit. Convective collapse of flux tubes. *Sol. Phys.*, 61:363–378, 1979. 18

H. C. Spruit. Dynamo action by differential rotation in a stably stratified stellar interior. *Astron. Astrophys.*, 381:923–932, January 2002. doi: 10.1051/0004-6361:20011465. 7

H. C. Spruit and E. G. Zweibel. Convective instability of thin flux tubes. *Sol. Phys.*, 62:15–22, 1979. 18

R. F. Stein and Å. Nordlund. On the formation of active regions. *Astrophys. J. Lett.*, 753:L13, 2012. 31, 32, 33

M. Stix. *The Sun. An introduction*. Springer-Verlag, Berlin, 1989. 2

P. A. Sweet. The Neutral Point Theory of Solar Flares. In B. Lehnert, editor, *Electromagnetic Phenomena in Cosmical Physics*, volume 6 of *IAU Symposium*, page 123, 1958. 12

R. J. Tayler. The adiabatic stability of stars containing magnetic fields-I.Toroidal fields. *Month. Not. Roy. Astron. Soc.*, 161:365, 1973. doi: 10.1093/mnras/161.4.365. 7

J. Warnecke, I. R. Losada, A. Brandenburg, N. Kleeorin, and I. Rogachevskii. Bipolar magnetic structures driven by stratified turbulence with a coronal envelope. *Astrophys. J. Lett.*, 777:L37, August 2013. 30

J. Warnecke, I. R. Losada, A. Brandenburg, N. Kleeorin, and I. Rogachevskii. Bipolar region formation in stratified two-layer turbulence. *ArXiv:1502.03799*, February 2016. 30

R. K. Yadav, T. Gastine, U. R. Christensen, and A. Reiners. Formation of starspots in self-consistent global dynamo models: Polar spots on cool stars. *Astron. Astrophys.*, 573:A68, January 2015. doi: 10.1051/0004-6361/201424589. 47

E. Yordanova, A. Balogh, A. Noullez, and R. von Steiger. Turbulence and intermittency in the heliospheric magnetic field in fast and slow solar wind. *Journal of Geophysical Research (Space Physics)*, 114:A08101, August 2009. doi: 10.1029/2009JA014067. 3

E. Yordanova, S. Perri, and V. Carbone. Reduced magnetic helicity behavior in different plasma regions of near-Earth space. *Journal of Geophysical Research (Space Physics)*, 116:A07230, July 2011. doi: 10.1029/2010JA015875. 3

U. Ziegler. A central-constrained transport scheme for ideal magnetohydrodynamics. *Journal of Computational Physics*, 196(2):393 – 416, 2004. ISSN 0021-9991. doi: http://dx.doi.org/10.1016/j.jcp.2003.11.003. URL `http://www.sciencedirect.com/science/article/pii/S0021999103006028`. 26

E. G. Zweibel and M. Yamada. Magnetic Reconnection in Astrophysical and Laboratory Plasmas. *Ann. Rev. Astron. Astrophys.*, 47:291–332, September 2009. doi: 10.1146/annurev-astro-082708-101726. 12, 14